RSC Advances

REVIEW

View Article Online
View Journal | View Issue

Check for updates

Cite this: *RSC Adv.*, 2022, **12**, 12166

Exploring the emerging applications of the advanced 2-dimensional material borophene with its unique properties

M. Bhavyashree,[acd] Sachin R. Rondiya[b] and K. Hareesh *[acd]

Received 1st February 2022
Accepted 28th March 2022

DOI: 10.1039/d2ra00677d

rsc.li/rsc-advances

Borophene, a crystalline allotrope of monolayer boron, with a combination of triangular lattice and hexagonal holes, has stimulated wide interest in 2-dimensional materials and their applications. Although their properties are theoretically confirmed, they are yet to be explored and confirmed experimentally. In this review article, we present advancements in research on borophene, its synthesis, and unique properties, including its advantages for various applications with theoretical predictions. The uniqueness of borophene over graphene and other 2-dimensional (2D) materials is also highlighted along with their various structural stabilities. The strategy for its theoretical simulations, leading to the experimental synthesis, could also be helpful for the exploration of many newer 2D materials.

Open Access Article. Published on 21 April 2022. Downloaded on 2/8/2026 10:57:22 PM.
This article is licensed under a Creative Commons Attribution-NonCommercial 3.0 Unported Licence.

1. Introduction

Graphene, a 2-dimensional material first invented by Novoselov and Geim,[1] has brought about a new era for the 2D material-based world towards the next-generation electronic devices and energy conversion devices.[2] Though it is yet to be materialized further, it has triggered the motivation that has led to the discovery of various 2D materials, either predicted theoretically or synthesized experimentally, for many potential electronic applications.[3] Moreover, on comparison with the bulk materials, the larger surface area, linear band structures, as well as enhanced quantum confinement effect of monoatomic layered 2D nanosheets,[4,5] have furnished their wonderful properties including high mobility, electronic properties such as metallicity, Dirac–Fermi effect and conductivity, which include AC conductivity, DC conductivity, optical conductivity and ultra-high thermal conductivity, mechanical properties such as excellent flexibility and high mechanical toughness and magnetic properties such as conductivity.[6,7] These properties have led to the potential applications of 2D nanosheets in energy storage, spintronics, photonics, electronics, sensing, biomedical fields, *etc.*[8,9] The other 2D compounds shown in Fig. 1(a) include, transition metal dichalcogenides (TMD),[10,11] boron nitrate (BN),[12] black phosphorous[13] and Xenes [X= As, B,

[a]*School of Applied Sciences (Physics), REVA University, Bengaluru-560064, India. E-mail: appi.2907@gmail.com*
[b]*School of Chemistry, Cardiff University, Cardiff CF10 3AT, Wales, UK*
[c]*Department of Physics, R.V. College of Engineering, Bengaluru-560059, India*
[d]*Center of Excellence on Macro-Electronics, Interdisciplinary Research Center, R.V. College of Engineering, Bengaluru-560059, India*

Miss Bhavyashree received her BSc degree (2017) in Physics, Chemistry and Mathematics, and MSc degree (2019) in Physics from Maharani's Science College for Women, Mysore, India. Her research interests are mainly focused on nano composite for field emission applications.

Dr Sachin R. Rondiya obtained his PhD (2017) from Department of Physics, Savitribai Phule Pune University, Pune, India. Later he joined Institute of Nano Science and Technology (INST), Mohali, Punjab, India as Post-Doctoral Fellow (2018–2019). Currently, he is a Post-Doctoral Research Associate in School of Chemistry, Cardiff University, Cardiff, United Kingdom. His research work focuses on developing nanoscale semiconductors for energy conversion and energy storage applications.

© 2022 The Author(s). Published by the Royal Society of Chemistry

Open Access Article. Published on 21 April 2022. Downloaded on 2/8/2026 10:57:22 PM.
This article is licensed under a Creative Commons Attribution-NonCommercial 3.0 Unported Licence.

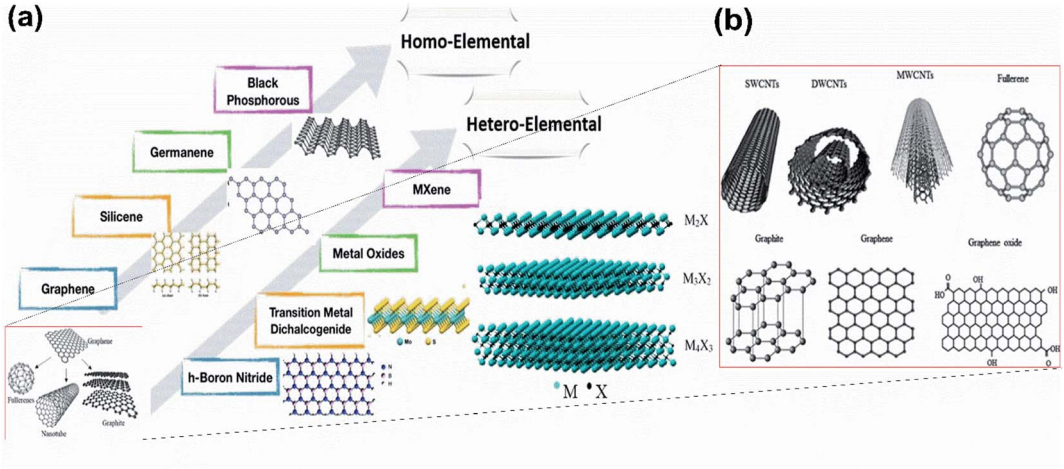

Fig. 1 (a) Existing homo-elemental and hetero-elemental 2D materials. (Reproduced from ref. 33 with permission from John Wiley and Sons). (b) Different shapes formed by graphene. (Reproduced from ref. 34 with permission from Elsevier).

Ge, P, Sn, Si, Sb].[14–20] The material field has made great strides through the emergence of one of the 2D materials, graphene, due to its ability to form spheres, tubes, sheets and a variety of curious shapes (Fig. 1(b)); however, its zero-band gap has interrupted many existing applications in photodynamic therapy, bio imaging, logic circuits, photonic devices and electronic components.[21] Hence there is the need for alternative 2D materials that could be more advanced as compared to graphene but with similar excellent properties such as high thermal conductivity, electrical conductivity, elasticity, flexibility, hardness and resistance, along with the ability to generate electricity when exposed to light and less effect towards ionizing radiation, low Joule effects (*i.e.* heating when conducting electrons) and electricity consumption, however, they must have an opening in their bandgaps. Among the previously studied 2D materials, the single-element materials are much more compatible with the previous technology of semiconductors, *i.e.*, Si and Ge, and are relatively easier to apply in high-quality synthesis and for decomposition and metabolization by the biological systems. For example, one of the monoelemental 2D nanomaterials, black phosphorous, has good biocompatibility and can easily decompose into phosphate, which could be useful for maintaining the physiological activities of DNA and ATP when used as raw materials. Additionally, the high specific area along with different response levels make these single-element 2D materials favourable candidates for various fields.[22–24] Among them, the recent interest is towards the mono layered boron allotrope, *i.e.* borophene, because, it not only has unique anisotropic, elastic, electronic, optical, superconducting, thermal and transport properties[25–27] but also impresses by its surface properties, electronic conductivity and unique chemical structures[28,29] due to the deficiency of electrons and multiple forms of chemical bonding, with two-electron bonds ranging from two-center to multicenter,[30–32] leading it to form a diversity of crystalline structures on varying the conditions and the method of synthesis. *Pmmn* borophene, α borophene and β_{12} borophene are predicted to exhibit different properties, where *Pmmn* is a Dirac material with novel electrical characteristics and Dirac cones, α is isotropic, whereas β_{12} is anisotropic,[21] indicating that any condition for the required applications could be met by regulating and controlling the preparation conditions. As such, this material requires much more exploration.

Boron is the fifth chemical element of the periodic table, which has valence orbitals like that of carbon (Fig. 2(a, e)) and is the only group 13 (*i.e.*, 3A) element with semiconducting properties.[35] For this reason, its 2D form, "Borophene", also possesses similar characteristics to that of graphene (*i.e.*, a 2D allotrope of carbon)[36,37] but has unique polymorphism in contrast to other 2D single-element materials.[38–40] Although boron is one of the nearest neighbours of carbon in the periodic table and has similar physical properties, its structure differs from that of graphene due to the difference in their degrees of buckling in the out-of-plane direction (as observed in Fig. 2(b, c and f, g)).[41] However, for a buckled borophene with triangular lattice, an important role is played by hydrogen as an acceptor[42] as it includes a system that has a surplus of electrons, and after

Dr Hareesh received his PhD (2014) from Mangalore University, India followed by Post-Doctoral Fellowship (2013–2017) from Savitribai Phule Pune University, India and University of Western Australia, Australia. Currently, he is an Assistant Professor in Physics at R.V. College of Engineering, Bangalore, India. His research interest includes 2D-based nanocomposites with transition metal oxides and conducting polymer for energy storage and energy conversion application.

Open Access Article. Published on 21 April 2022. Downloaded on 2/8/2026 10:57:22 PM.
This article is licensed under a Creative Commons Attribution-NonCommercial 3.0 Unported Licence.

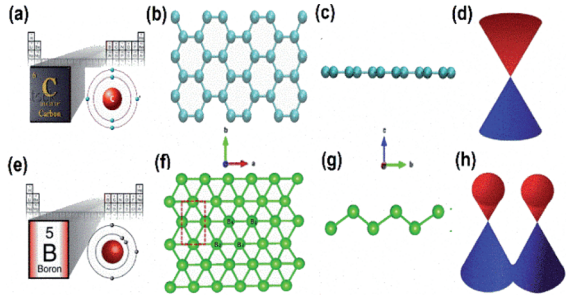

Fig. 2 Schematic representation of the valence electrons of (a) carbon and (e) boron respectively in their similar orbital. (Reproduced from ref. 27 with the permission of Elsevier), graphene with (b) top view, (c) side view (reproduced from ref. 46 with the permission of American Physical Society), (d) graphene Dirac cone, borophene (f) top view and (g) side view (reproduced from ref. 31, published by IOP Publishing Ltd, licensed under Creative Commons Attribution 3.0) and (h) Dirac cone of borophene (reprinted with permission of ref. 3. Copyright (2020) Wiley-VCH Verlag GmbH).

hydrogenation a linearly dispersed Dirac cone as observed in Fig. 2(h), similar to that of graphene in Fig. 2(d), arises in the resulting borophene.[43] For this reason, there is still the need for more research on the allotropes of borophene. However, theoretical simulations from the 1990s have revealed interesting properties related to different low-dimensional borophene allotropes.[44] Its synthesis in 2015 *via* the condensation of atoms of hot boron gas on a cool silver surface forced the creation of its hexagonal structure because of the regular silver arrangement. However, the notable proportions of silver and boron (B) atoms have led to the creation of vacancies or holes in the lattice and these vacancy patterns provide unique properties for the borophene crystal.[45]

Unlike all other direct experimentally synthesized traditional materials, the borophene design began through theoretical simulations[47–49] with the predictions of their probable characteristics,[50–52] followed by preparation methods, and then their synthesis in laboratories and their potential applications. This unique strategy is schematically represented in Fig. 3(a),[53] and the yearly progress in the publication of borophene papers, is plotted in Fig. 3(b). This emerging development of borophene could be a model for various new materials and a best example for the material genome project (MGI),[21] which can improve the synthesis efficiency, minimize the research material cost and increase the material design output rate.

This paper provides useful information regarding the progress of borophene through previous simulation analyses, experimental confirmation, and different mechanisms for laboratory synthesis. We also report a few of their properties, including the factors that can cause alterations, make comparisons with other 2D materials, and explore their existing applications with updated information to guide researchers in identifying further challenges, and provide opportunities for improvement in various other fields.

2. History of theoretical prediction before experimental confirmation

Until 2015, experimental research on allotropes of nanostructured boron was very sparse due to their toxic and costly precursor (diborane), which was typically suggested.[45] However, in the 1990s, using computer simulations, a physicist, I. Boustani, first examined the structure of tiny boron clusters on studying their stability and reported that the final structures mostly preferred the quasi-planar or planar form rather than the icosahedral geometry like that of borane.[48] Computational studies have suggested various structures for the 2-dimensional boron sheet[50] but in accordance with the general class of quasiplanar clusters of B_7 [Fig. 4(a)], Boustani proposed the aufbau principle (inset of Fig. 8(a))[47] for constructing nanostructures, which predicted the possibilities of fullerenes of boron (borospherene),[55] boron nanotubes[30,56,57] and monoatomic sheets of boron (borophene) (Fig. 4(d–f)).[49] Since the monoatomic sheet of boron was 2-dimensional and as the traditional rule suggests

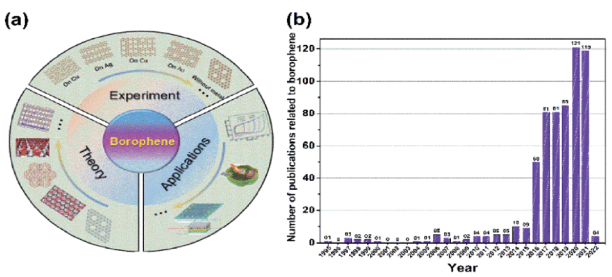

Fig. 3 (a) Schematic diagram of the development of borophene. (Reproduced from ref. 54 with the permission of John Wiley and Sons). (b) The number of publications focusing on borophene each year. (From the web of sciences, https://publons.com/publon/).

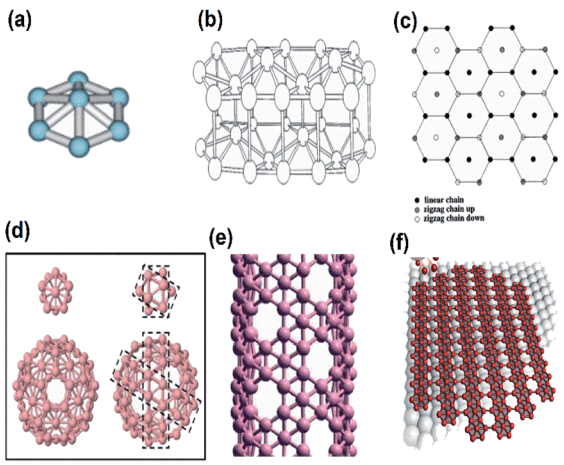

Fig. 4 Boron allotropes: (a) quasi-planar cluster of B_7 (reproduced from ref. 62 with the permission of Elsevier). (b and c) A double-layered boron cluster, side view and top view, respectively (reproduced from ref. 61 with the permission of AIP Publishing). (d) Fullerene of boron (reprinted with permission from ref. 60. Copyright (2019) Wiley-VCH). (e) A boron nanotube (reprinted with permission from ref. 63. Copyright (2008) American Physical Society). (f) Monoatomic sheet of boron (reproduced from ref. 53, Science and Technology review publishing house licensed under Creative Common Attribution 4.0 international).

© 2022 The Author(s). Published by the Royal Society of Chemistry

Open Access Article. Published on 21 April 2022. Downloaded on 2/8/2026 10:57:22 PM.
This article is licensed under a Creative Commons Attribution-NonCommercial 3.0 Unported Licence.

the fundamental name for the 2-dimensional materials to be 'Xene', where X is the element, the monoatomic sheet of boron was named as "Boronene".[58] Further, after analysing the graphene and its aromatic rings of carbon atoms, a monolayer sheet was introduced for the B atoms as well and was called "Borophene". However, those sheets gave high stability when enhanced by the out-of-plane distortion[39,59] or by superstructures of vacancies.[30,50] This was because, as a contradiction to graphene, the valency of boron was only three, and it was deficient of a single electron to make sp^2 bonding and form a hexagonal lattice as graphene, hence a planar triangular lattice was proposed in the beginning.[60] Later, Boustani noticed that the planar triangular lattice was not stable and put forth a buckled structure, *i.e.*, a distortion along its out-of-plane direction from the model of clustered boron in two layers, which consisted of zigzag chains of boron in the up-down direction as seen in Fig. 4(b and c), where its energy for each atom was 0.03 eV lower than the unbuckled one and 0.7 eV lower than the graphene-like honeycomb lattice.[61]

In 2005, advanced buckled structures were proposed for borophene as seen in Fig. 5(a–d) and it was determined that the p-orbital symmetries of the B atom were not agreeable with the six-fold coordination in the flat borophene triangular lattice. Hence, *via* σ–π bond mixing, a buckled structure termed buckled {1212} boron sheet (δ_6 borophene) was formed, enhancing the cohesive energy, and when compared with the single-atomic strength of the flat one, it was 0.26 eV stronger.[64] In δ_6 borophene two different B–B bonds of bond length 1.81 and 1.63 Å were formed, where the height of buckling was ~0.85 Å.[65] Further, *ab initio* structural optimization disclosed that any random lattice of buckled triangles would relax into δ_6 borophene, indicating it as the best structure. Different configurations of borophene including planar reconstructed {1212}, idealized buckled {1212}, icosahedral (bulk boron with α-phase) and few low-symmetry hybrid structures were investigated and among them the most stable structure was the one highlighted in Fig. 5(b), *i.e.*, the buckled {1212}.[59]

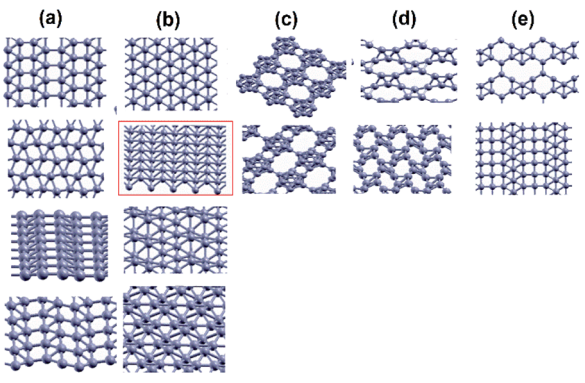

Fig. 5 Advanced buckled structures: (a) reconstructed {1212}, (b) idealized and buckled {1212} with the stable one marked in red, (c) icosahedral boron, (d) lower symmetry and (e) few hybrids. Reprinted with permission from ref. 59 Copyright {2007} American Chemical Society.

As mentioned previously, the proposed triangular lattice structure, due to the electron deficiency in boron,[63,66] can form multicenter-two-electron bonds for stabilizing the structure by buckling.[30,67] Later, it was found the flat triangular structure had an excess of electrons, while the hexagonal structure was highly unstable due to the shortage of electrons and for decreasing the energy it requires more electrons. Hence, a mixture of hexagonal lattice, *i.e.*, acceptors and trigonal lattice, *i.e.*, donors, was proposed, which gave rise to triangular motifs of borophene having hexagonal holes[30] and predicted that the superstructure vacancies could also improve the stability of the previously proposed flat triangular lattice of borophene. Moreover, a greater cohesive energy was noticed for the hexagonal vacant triangular sheet than the previous one without hexagonal holes.[54] This then gave rise to the density parameter,[21] based on this, the concentration of hexagonal vacancies could be varied in the motif, where the density parameters were found to be $\eta = 0$ and $\eta = 1/3$ for triangular and hexagonal sheets, respectively. Depending on the same, various configurations were formed as in Fig. 6(a) but more stability was noted in $V_{1/9}$ ($\eta = 1/9$) and $V_{1/7}$ ($\eta = 1/7$) structures, also termed α-borophene and β-borophene, respectively.[21,30,68] Analysis of the calculated band structure of $V_{1/9}$, designated α-borophene to be metallic[63] with the highest cohesive energy/atom.[30] A new borophene structure similar to that of α-borophene was proposed with hexagonal holes in parallel and was denoted as the γ-sheet (B_{36}). This γ-sheet was ultra-stable, especially for the B_{100} cage (highlighted in Fig. 6(b)).[69] However, in 2014, based on the outcomes of photoelectron spectroscopy and the simulations of theoretical data, there was a first report on the experimental discovery that the B_{36} boron cluster was quasiplanar with high reliability and consisted of a predominant hexagonal hole and hence it was potentially viable for reproducing sheets of single-atomic layered boron on a larger scale with hexagonal vacancies.[50]

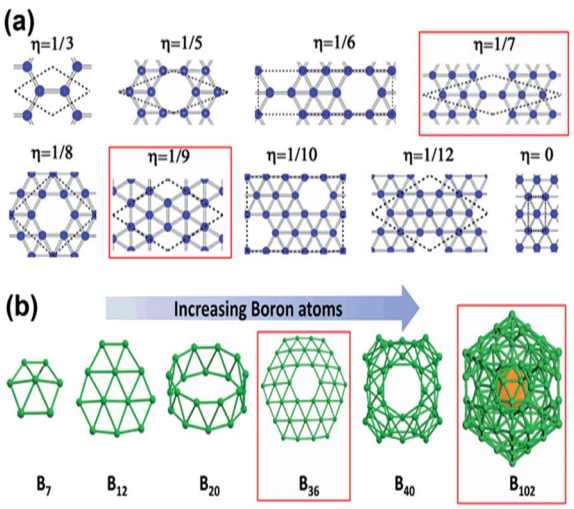

Fig. 6 (a) Various density parameter-dependent configurations with two stable structures marked in red. (Reproduced from ref. 70 with the permission of AIP Publishing). (b) Structural variation with an increase in the number of boron atoms. (Reproduced from ref. 58).

Open Access Article. Published on 21 April 2022. Downloaded on 2/8/2026 10:57:22 PM.
This article is licensed under a Creative Commons Attribution-NonCommercial 3.0 Unported Licence.

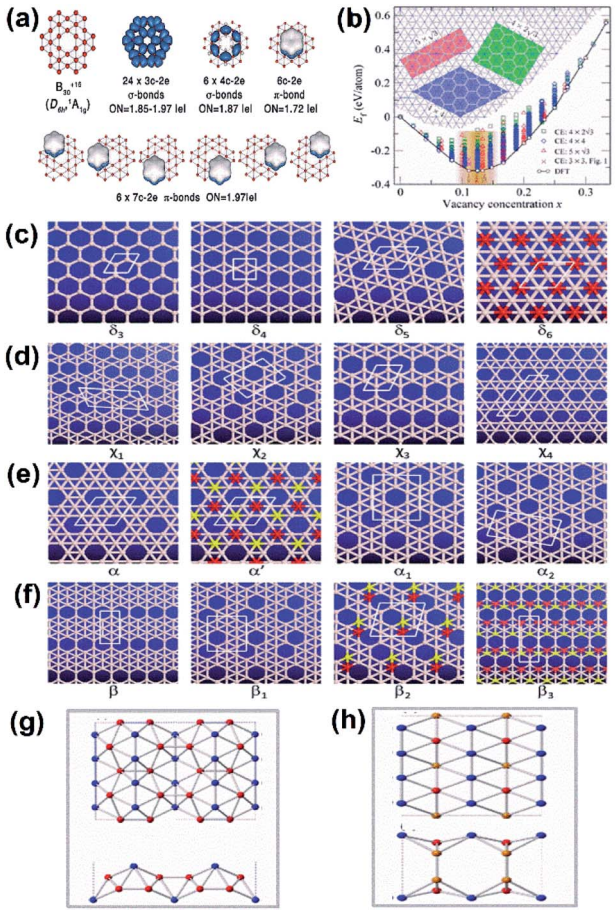

Fig. 7 Complexes of borophene: (a) *n*-center, 2-electron (reproduced from ref. 71 with the permission of the Royal Society of Chemistry), (b) cluster expansion (CE) method (reprinted with permission of ref. 72. Copyright (2012) American Chemical Society), (c–f) CALYPSO code (reprinted with permission from ref. 74 Copyright (2012) American Chemical Society), (g, h) buckled structures with small thicknesses and 2 × 2 × 1 supercell projections along [001] and [100] for (g) *Pmmn*-boron and (h) *Pmmm*-boron. (Reprinted with permission from ref. 60. Copyright (2019) Wiley-VCH).

$$\eta = \frac{\text{No. of holes of hexagon}}{\text{No. of atoms in basic triangular sheet}}$$

A better understanding of α-borophene was given by Galeev *et al.*[71] by reporting about its fragments along with chemical bonding, wherein an adaptive natural density partitioning (AdNDP) method was used. As seen in Fig. 7(a) α-borophene was classified with regard to '*n*'center-2 electrons, where $n = 2,3$ and 4 in σ-bonds and $n = 6$ and 7 in π-bonds, but there was instability in the borophene structure when the σ : π electron ratio was 0.5.[71] Subsequently, various possible borophene structures, as seen in Fig. 7(b), were constructed by the cluster expansion (CE) method and named $B_{1-x}\hexagon_x$, with ⬡ as the hexagonal vacancy. Those configurations were different in structure, dependent on $x = 0.1$–0.15 but they had nearly similar energy formations, especially for borophenes with $x = 1/9$, 1/8 and 2/15, which were also analyzed as shown in Fig. 7(b). At room temperature, on taking KBT = 0.026 eV, the substrate-independent borophene mostly preferred to have a polymorphic structure.[72] As seen in Fig. 7(c–f) several complexes of borophene were predicted *via* the swarm optimization (CALYPSO) code, and the α-sheet was the ground state among the independent borophenes.[73] Since the energy difference was very narrow between $V_{1/8}$, $V_{2/15}$ and α($V_{1/9}$)-borophene, GGA-PBE was less effective for ensuring their relative stability, hence their cohesive energy was calculated using a hybrid functional PBE0,[74] where α_1-borophene showed 136 meV per atom higher energy than the α-sheet, and β_1-borophene showed 118 meV per atom and 96 meV per atom high stability than the β-sheet and α-sheet, respectively. However, $V_{1/8}$ and $V_{2/15}$ had approximately the same cohesive energy and were much more stable (*i.e.*, 30 meV per atom) than α-borophene.[30,74,75] Hence, the α-sheet, previously trusted as the ground state, was proven wrong.

Besides these, two more buckled structures, having non-zero thicknesses, namely *Pmmn* (Fig. 7(g)) and *Pmmm* (Fig. 7(h)), were also predicted. The results of the HSE06 (GGA-PBE) calculation showed the ultra-stability of the *Pmmn*/*Pmmm* sheet as compared to the α-sheet but their stability relations are yet to be studied. The *Pmmn* phase having low symmetry with the linearity of the Dirac dispersion similar to graphene was identified to be semi-metallic.[39] All these predictions were only for the substrate-independent borophene and all of them showed perfect single-crystallinity. Nevertheless, substrate-supported borophene varied in stability and offered many more new, mixed structures.

The dynamical instability in the proposed freestanding borophene[32] motivated many researchers to find various methods for improving their stability, which included surface functionalization and adsorption on substrates.[28,32,76,77] After analyzing the growing mechanism of graphene and silicene on the metal surface, the metal-based substrates were regarded to be a productive way for finding the solution for borophene sheets.[54] Through theoretical calculations, numerous 2-dimensional boron allotropes in Fig. 8(a) were reported,[36,67,78,79] wherein the computational studies by Liu *et al.*[80] proved that they could be extracted by the deposition of boron sources on the substrates of Au, Ag, Cu or metal bromides (MgB_2).[80] Again, using swarm optimization (CALYPSO), numerous complexes were predicted on the surface of Ag/Au/Cu/Ni and their results in Fig. 8(b) indicated their structural variations at the respective ground states for different metal substrates. Later, on identifying a large difference in the lowest energies of the two structures formed on Cu, $V_{1/6}$ sheets, *Pmmm* were found to be much more stable on Cu.[81] It was also found that resultant 2D boron clusters on Cu(111) contained holes and it was observed that nucleation of the 2D cluster by Cu substrate could easily form hexagonal holes.[82] This was an essential framework that led to other successive theoretical predictions. Further, based on the first principles calculation *via* surface structure search and the CE method, the borophene sheets were systematically investigated and resulted in a hexagonal-holed triangular pattern when grown on Cu, Au, Ni and Ag, where icosahedral β_{12} was not favorable on Ni and Cu but was minimum on Au and Ag, which indicated that those metals could promote the

© 2022 The Author(s). Published by the Royal Society of Chemistry

Open Access Article. Published on 21 April 2022. Downloaded on 2/8/2026 10:57:22 PM.
This article is licensed under a Creative Commons Attribution-NonCommercial 3.0 Unported Licence.

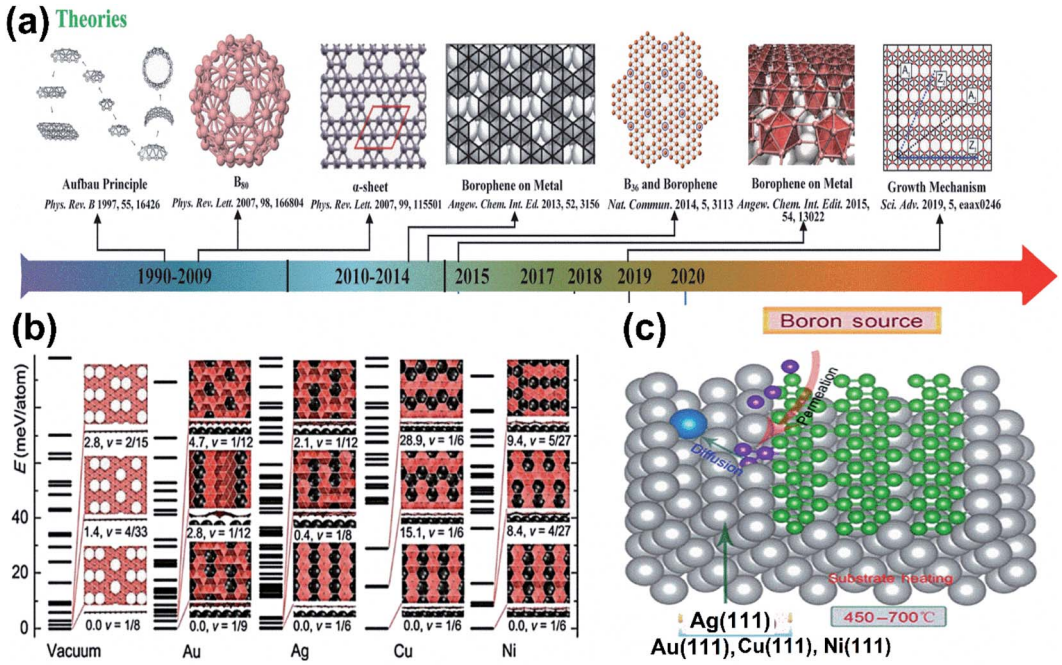

Fig. 8 (a) Theoretically simulated borophene structures with yearly categorization. (Reproduced from ref. 54 with the permission of John Wiley and Sons). (b) Stability *versus* hole density under vacuum and on Au, Ag, Cu and Ni substrates with structures formed at their different energy states. (Reprinted with permission ref. 81 Copyright 2015, Wiley-VCH). (c) Schematic representation of boron sheet nucleation over the metal substrate for its stabilization, (reproduced from ref. 83).

nucleation as represented in Fig. 8(c) within boron sheets and donate extra electrons for stabilizing it.[81] Successively, the predictions were experimentally confirmed initially in the same year (2015) by Mannix *et al.*,[45] using Ag(111) as the metal substrate.[45] Furthermore, corresponding experiments on same substrate showed that it could cause nucleation and donate electrons for stabilization and reported β_{12} ($\eta = 1/6$) to be the ground state.[15] Presumably, under ultra-high vacuum conditions, four phases of borophene, namely the 2-*Pmmn* phase, β_{12} phase, χ^3 phase and graphene-like honeycomb phase were developed successfully on Al/Ag/Au/Cu(111) substrates,[15,51,53] which are discussed in detail in Section 3.

3. Synthesis of 2D borophene

The 3D boron bonding configurations,[32] accompanied by a large difference in energy as compared with the 2D form,[84] make the fabrication of borophene a challenging task. Usually, this requires ultralow pressures and sophisticated facilities for its fabrication.[3] Even then, on considering the theories, borophene synthesis was possible *via* the bottom-up approach,[15,18,45,85] top-down approach,[86–88] exfoliation techniques (*i.e.*, sonochemical, liquid phase),[87–89] deposition techniques (*i.e.*, CVD, PVD)[32,90–92] *etc.* It gave raise to different complexes of borophene, which were either supported by a substrate, or independent (*i.e.*, freestanding) one.[93]

3.1. Growth of borophene supported on a substrate

Due to the presence of periodic hexagonal holes in borophene or hexagonal boron (highlighted in Fig. 6(b)) within its triangular lattice, theoretically, it was very stable[63] when supported on metal substrates such as aluminium Al(111),[94] silver Ag(111),[15,45] gold Au(111)[95] or copper Cu(111).[82,96] This was achieved through various fabrication methods such as atomic layer deposition, molecular beam epitaxy, chemical vapor deposition, and so on. The merit of these method includes the chemical purity of the obtained borophene for the further study of the chemical and physical behaviours.

3.1.1. Atomic layer deposition (ALD). Atomic layer deposition, being an ultra-thin film deposition technique with high quality, was the first synthesis technique employed for growing atomically thin borophene sheets on a clean single-crystal surface of inert Ag(111) by Mannix *et al.*[45] The sheets were developed by using solid boron as an atomic source, under ultrahigh-vacuum as shown in Fig. 9(a). This resulted in three phases of borophene, namely, stripped phase, homogeneous phase and nanoribbons (Fig. 9(b)), at the substrate temperature of 550 °C. The scanning tunnelling microscopy (STM) results represented in Fig. 9(c–h) also disclosed that at a lower deposition rate, there appeared a flat strip as shown in Fig. 9(b), which consisted of a rectangular lattice with hollow hexagons, whereas a high deposition rate gives a homogeneous phase as in Fig. 9(b). As the temperature increased, the flat phase appeared as a conjugated striped phase in Fig. 9(b) but both phases showed metallic characteristics.[45] However, the ultra-high vacuum condition provision in laboratories is costly and challenging and the process was time consuming with high material use, as well as energy wastage.

3.1.2. Molecular beam epitaxy (MBE). Borophene was experimentally realized by molecular beam epitaxy (MBE) in

Open Access Article. Published on 21 April 2022. Downloaded on 2/8/2026 10:57:22 PM.
This article is licensed under a Creative Commons Attribution-NonCommercial 3.0 Unported Licence.

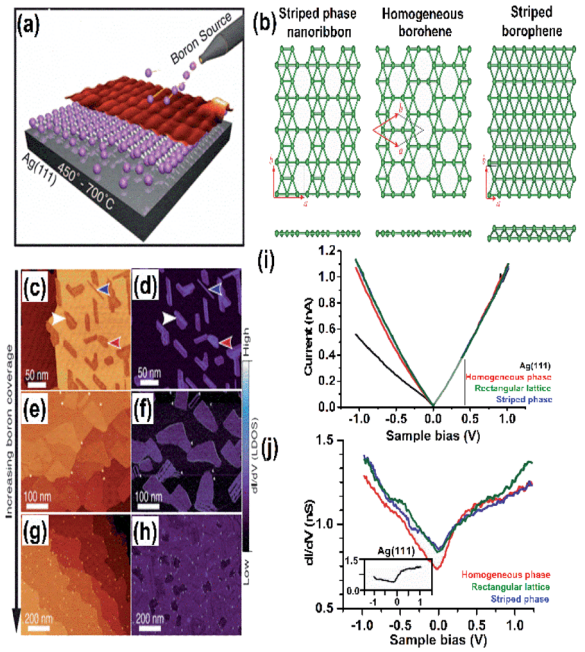

Fig. 9 (a) Schematic representation of the atomic layer deposition of boron on Ag(111), (b) three phases formed at 550 °C (reproduced from ref. 97, published by Taylor & Francis Group, licensed under Creative Common Attribution). (c–h) Series STM topography in large-scale (on left) and d*I*/d*V* closed-loop (on right) images for the borophene sheets, where (c and d) shows low coverage of boron, (e and f) medium coverage of boron, (g and h) high coverage of boron, with blue, red and white arrows indicating the striped phase nanoribbon, homogeneous-phase and striped phase of borophene (reproduced from ref. 21, published by Wiley-VCH GmbH, licensed under Creative Common Attribution 4.0 International). (i and j) *I*–*V* curve and d*I*/d*V* spectra indicating the metallic characteristics of the resulting boron sheets. (Reproduced from ref. 53. Published by Science and Technology Review publishing house, licensed under Creative Commons attribution 4.0 international).

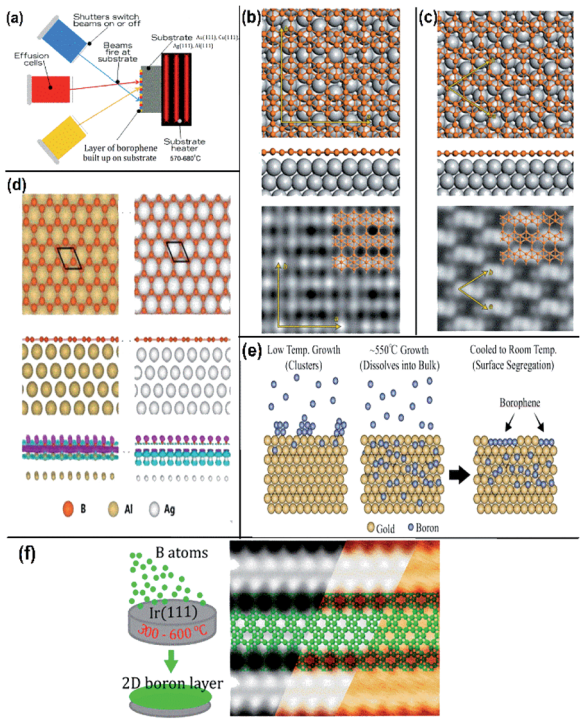

Fig. 10 (a) Schematic MBE method representation, (Published by GO LOOK IMPORTANTBOOK), (b and c) (from top to bottom) top view, side view and STM image of (b) β_{12} and (c) χ^3 on Ag(111), (reproduced with the permission of ref. 25. Copyright (2019) Wiley-VCH Verlag GmbH) (d) borophene (honeycomb structure) on Ag(111) and Al(111) represented with different colours as mentioned (from top to bottom) top view, side view and the electron density map, (reproduced from ref. 51 with permission of Elsevier). (e and f) Schematic borophene growth on (e) gold substrate, (reprinted with permission from ref. 95. Copyright (2019) American Chemical Society) and (f) iridium substrate with its STM image (reprinted with permission from ref. 100, Copyright (2019), American Chemical Society).

2016, and it can also be grown epitaxially on the substrate Ag(111). The boron sheets were grown in ultrahigh vacuum conditions on Ag(111) by directly evaporating the pure boron using the mechanism of molecular beam epitaxy (MBE), as shown in Fig. 10(a). It was S confirmed that two different 2-dimensional patterns of boron sheets were formed successfully on the Ag(111), namely sheets of β_{12} (Fig. 10(b)) and sheets of χ^3 (Fig. 10(c)). The results revealed a new application in micro-electronic appliances and proposed that materials like Au(111), Cu(111) and metal borides can be further employed as the substrates instead of Ag(111), where the MBE method could result in extremely pure/clean borophene.[15] Li *et al.*[51] and Kiraly *et al.*[95] used metal substrates with low surface energy, *i.e.*, Al(111) and Au(111), respectively, to grow the borophene *via* the MBE method. The obtained honeycomb structural borophene on Al(111) was much more stable than the one grown on Ag(111), which allowed the fabrication of extremely thin films. By logical calculations, it was manifested that a charge of around 1 eV was transferred from the Al to each of the B atoms in the honeycomb borophene, which stabilized the borophene/Al(111) structure in contrast to borophene/Ag(111) because the charge transfer within it was negligible (Fig. 10(d)).[51] In the borophene/Au(111) synthesis procedure as demonstrated in Fig. 10(e), at higher temperatures, the B atoms diffuse into gold and when allowed to cool, those B atoms become separated on its surface, giving rise to boron sheets. Further, on increasing the B concentration, the initially trigonal Au(111) network breaks, resulting in a large-scale borophene island and can extend to several nanometres on increasing the boron dose *via* electron-beam evaporation.[95] Although MBE is a typical process for preparing substrate-supported borophene with high uniformity and fewer defects, an alternate method similar to MBE for borophene synthesis over mica[98] and Ir(111)[99] was reported *via* van der Waals epitaxial growth and segregation-enhanced epitaxial growth (schematically shown in Fig. 10(f)), respectively, which resulted in larger single-phased borophene. However, the process was a very slow and laborious method, *i.e.*, with a growth rate of a few microns per hour indicating the suitability of the MBE method for a scientific research laboratory rather than high-volume production. Further, on comparing the atomic structures obtained by ALD and MBE, it was reported to have a small difference in the densities of boron

© 2022 The Author(s). Published by the Royal Society of Chemistry

Open Access Article. Published on 21 April 2022. Downloaded on 2/8/2026 10:57:22 PM.
This article is licensed under a Creative Commons Attribution-NonCommercial 3.0 Unported Licence.

atoms.[3] However, the deposition of borophene is limited to small area *via* both methods, which could make the further fabrication of practical devices a challenging and costly task at the industrial scale.

3.1.3. Plasma-enhanced chemical vapor deposition (CVD). Of the modern methods for graphene synthesis, plasma-enhanced CVD is a distinct alternative to exfoliation.[101] This method enables various 2D material syntheses at the industrial scale without the requirement of high vacuum levels. Previously, with the help of catalytic substrates, CVD emerged as a convenient method for obtaining large-sized graphene with high-quality, in which graphene was obtained in the deposit form by suitable precursor decomposition when exposed to the substrate by controlling the pressure of the CVD system as represented in Fig. 11(a), which could be later transferred to various target substrates by a polymer-assisted transfer process as seen in Fig. 11(b).[91] As observed for silicene and graphene, CVD growth may improve the size of borophene laterally, resulting in a decrement of density defects along with an increment in borophene grain size,[91,102] which enable the researchers to study the advanced properties of borophene under intrinsic conditions. This method can even enhance the scalability of borophene. Moreover, the thin 2D γ-B film was synthesized by Tai *et al.*[92] *via* CVD using a copper foil substrate (Fig. 11(b–d)). The source was taken as a mixture of powdered boron oxide and pure boron, and hydrogen as the carrier gas. The temperature of the source region (T1) and substrate region (T2) was manipulated independently as 1100 °C and 1000 °C, respectively, in the CVD furnace.[92] However, a few reports have suggested that borophene growth *via* the CVD process requires the identification of a precursor for boron and an active catalyst for its decomposition, including the nucleation and growth of the 2D material. Another important fact is the identification of the growth of the non-metallic substrates, which facilitates the characterization of the lateral charge transport.[32] This method showed different chemical properties such as resistance to corrosion and high chemical and thermal stability. However, the process was very time consuming and required high-cost equipment and the resulting borophene was unstable against aging and humidity.

An improvement in the CVD technique was noticed when micrometer-sized borophene was grown over a thick Cu(111) film on sapphire, in which the boron was repeatedly submersed into the Cu at a high temperature, and at low temperature it was recrystallized and resurfaced. Through this technique, the size of the wafer was scalable, copper film could be relinquished and sapphire could also be reused.[96] Furthermore, an efficient technique namely, van der Waals epitaxy was used for growing borophene on a larger scale *via* CVD in a furnace with two zones. An additional intermediate of metastable boron cluster was formed by annealing sodium borohydride powder [$NaBH_4$] (*i.e.*, boron source), the polymer and substrate chosen were fluorophlogopite mica ($KMg_3AlSi_3O_{10}F_2$)[98] and polymethyl methacrylate (PMMA), respectively. Recently, CVD was employed for synthesizing borophene on Ni foil to get a semiconductor having a direct band gap with tunable properties.[98]

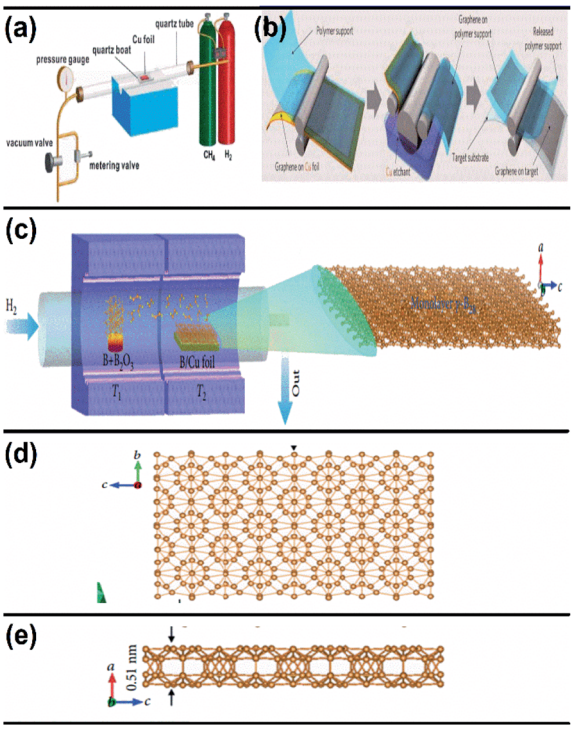

Fig. 11 Schematic representation of (a) the CVD graphene system at a controlled pressure, (b) the transfer of the synthesized graphene to the target substrate (reproduced from ref. 91 with permission from the American Chemical Society). (c) Diagram of the furnace with two zones for the growth of borophene on Cu *via* CVD. (d) Top view and (e) side view of the resultant borophene obtained in (c). (Reproduced from ref. 92 with permission of John Wiley and Sons).

3.2. Free-standing borophene sheets

Due to the myth that bulk boron forms non-van der Waals crystals,[103] the fabrication of free boron nanosheets is considered challenging; however, there have been a few recent findings on free-standing (*i.e.*, independent) borophene by methods like exfoliation and the modified Hummers' method, which have completely broken the myths.

3.2.1. Micromechanical exfoliation. Due to a network with complex bonding in boron, there are very few studies on undeviated exfoliation as a technique for the fabrication of borophene. However, borophene exfoliation employing solvents or chemicals resulted in defects/functionalities along with fragmented sheets with uniform layers and high quality.[103] The borophene synthesis was reported through three steps of a top-down approach (Fig. 12(a)), which included liquid exfoliation twice along with etching through thermal oxidation. At first, the exfoliation resulted in a thick boron nanosheet, which was oxidized to B_2O_3 and then dissolved in water. Subsequently, a boron nanosheet of less than 5 nm thick with 100 nm lateral size was obtained after ultrasonic exfoliation.[88] However, atomic borophene sheets were easily synthesized by exfoliation through a liquid-phase and proved the borophene oxide reduction as well. The existence of intermediate borophene phases along with β_{12} (Fig. 12(c)) and χ^3 (Fig. 12(d)) was verified

Open Access Article. Published on 21 April 2022. Downloaded on 2/8/2026 10:57:22 PM.
This article is licensed under a Creative Commons Attribution-NonCommercial 3.0 Unported Licence.

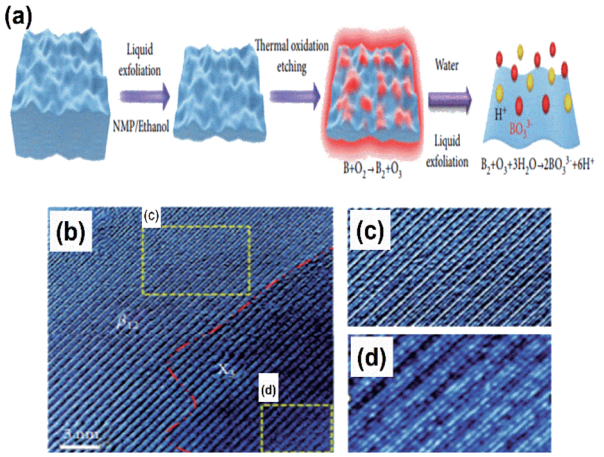

Fig. 12 (a) Schematic micromechanical exfoliation representation by the top-down approach. (b) Electron microscope image of the resulting borophene sheet. (c and d) Zoomed images of the (c) β_{12} and (d) χ^3 phases observed in (b) (reproduced from ref. 53 Published by the Science and Technology Review Publishing House licensed under the Creative Common Attribution 4.0 International).

by characterization using electron microscopy.[87] Further, as illustrated by Coleman *et al.*,[89] defect-free graphene was synthesized *via* liquid exfoliation of graphite and was used for a variety of applications. The ultrasonication of graphite powder in a suitable solvent (*i.e.*, dimethylformamide, deionized water, isopropyl alcohol, ethylene glycol, acetone, *etc.*) gave rise to a stabilized nanosheet. It was recommended that similar liquid-phase exfoliation be employed for the fabrication of defect-free borophene also.

Mixing the required nanosheet in a suitable solvent is given in terms of a thermodynamic equation:

$$\frac{\Delta H_{\mathrm{mix}}}{V_{\mathrm{mix}}} = \frac{2}{T_{\mathrm{B}}}\left((E_{\mathrm{S,S}})^{1/2} - (E_{\mathrm{S,B}})^{1/2}\right)^2 \varphi_{\mathrm{B}}$$

where ΔH_{mix} is the mixing enthalpy, V_{mix} is the mixture volume, T_{B} is borophene thickness, $E_{\mathrm{S,S}}$ is the solvent surface energy, $E_{\mathrm{S,B}}$ is borophene surface energy and φ_{B} is the dispersed borophene volume fraction. A small amount of external energy (sonication) would be enough for exfoliation if $E_{\mathrm{S,S}}$ and $E_{\mathrm{S,B}}$ are similar and borophene nanosheet structures were formed due to the relaxation of the developed local strain. They even proved that the atomic interaction of solvent with the borophene sheet is crucial to the process as their experimental trial suggested that acetone could yield the monolayer formation in the case of sonochemical exfoliation on behalf of other solvents.[1] Moreover, this method of synthesis helps in obtaining a larger lateral dimensioned monolayer, bilayer or tri-layer sheets on varying the frequency, time and amplitude of sonication as well as the chosen solvent. However, prolongated sonication can result in borophene dots rather than sheets and slight changes give a very different structure. Hence, the choice of an adequate and suitable solvent along with the sonication parameter is challenging, time consuming and crucial for obtaining the particular borophene sheets.

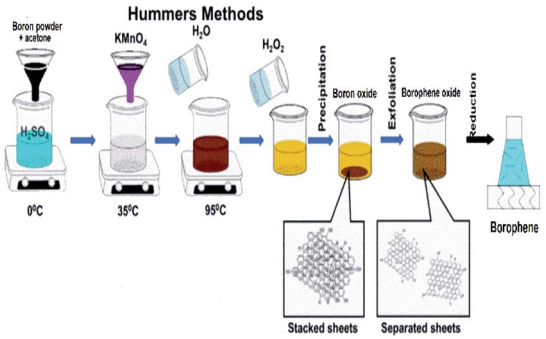

Fig. 13 Schematic representation of the modified Hummers' method. (Reproduced from ref. 104 published by MDPI, licensed under the Creative Commons Attribution).

3.2.2. Modified Hummers' method. The modified Hummers' method is one of the most commonly used methods for the synthesis of high-quality graphene. Introductory pure crystalline, free-standing sheets of large area borophene were obtained extensively by Ranjan *et al.*[93] through the modified Hummers' method when combined with sonochemical exfoliation as shown in Fig. 13. It showed that the potassium permanganate and boron ratio is also an important parameter during exfoliation. Borophene obtained through such a method was suitable for application in the sensing of gas, strain and molecules (*i.e.*, in surface-enhanced Raman spectroscopy). This even disproved the hypothesis that borophene would not exist in free-standing form and showed that a single chemical reaction can confirm the existence of β_{12} and χ^3, accompanied by their intermediate phases; the formation of these phases formation was governed by strain, interlayer interaction and the number of layers.[93] Although, the improved oxidation level obtained *via* the modified Hummers' method improves the product performances, the long-time taken for the complete process along with its tedious purification process revealed the complexity of the modified Hummers' method in borophene synthesis. A comparison of the merits and demerits of each method is given in Table 1.

On comparing the overall scalability of the process with that of graphene, it was revealed that an allotrope of carbon, *i.e.*, graphite, being the starting material of graphene, is a non-metallic and tetravalent element, which is the 15th most abundant element in the Earth's crust and the 4th most abundant element in the universe, hence is easily available in a larger quantity and has a wide application. However, boron, the starting material for borophene, occurs on the Earth in a significant concentration known as borate mineral, which is of 100 different types but the most common ones are borax, kernite and ulexite; their cost is ten times higher when compared to that of graphite.

4. Properties

Given the interesting facts about borophene, its promising contribution is suggested for sensing and electronic applications, hence numerous studies have been devoted to

© 2022 The Author(s). Published by the Royal Society of Chemistry

Open Access Article. Published on 21 April 2022. Downloaded on 2/8/2026 10:57:22 PM. This article is licensed under a Creative Commons Attribution-NonCommercial 3.0 Unported Licence.

Table 1 Comparison of merits and demerits of different methods of borophene synthesis

	Method	Merits	Demerits	References
Substrate supported	Atomic layer deposition	• High-quality ultra-thin film • Excellent repeatability • High film density • Large area thickness uniformity • Atomically flat and smooth surface coating • Low-temperature processing	• Time consuming chemical reaction • Very high material and energy waste rate • Obtaining ultra-high vacuum condition is challenging and costly	45
	Molecular beam epitaxy	• Extremely pure/clean borophene • Ultra-thin film • High uniformity with less defect	• Very slow and laborious method. *i.e.* growth rate few micrins per hour	15, 51 and 95
	Plasma enhanced CVD	• Industrial scale synthesis possible • No requirement of high vacuum level • High thermal and chemical stability • Corrosion-resistant	• Time-consuming • Costly equipment • Instability to humidity	32, 91, 92, 96, 98, 101 and 102
Freestanding	Micromechanical exfoliation	• Uniform layered high quality • Larger lateral dimensions with different layers	• Slight changes in conditions/ parameters cause irreversible changes in the structure • Choice of suitable and adequate solvent is tedious	88, 89, 103 and 104
	Modified Hummers' method	• Oxidation level improved • Enhanced product performance	• Time-consuming process • Tedious purification process	93

understanding borophene's properties and structure. A detailed discussion regarding a few major properties such as high mechanical properties, electronic or ionic conductivity, lattice thermal conductivity, super conductivity, optical properties, atomic adsorption, surface reactivity and high capacity are mentioned in some of the review articles.[3,53,54,105]

After understanding the borophene structure as discussed in Section 2 it is important to introduce its properties. The natural 3D boron structure indicates that it is an intermediate of both metals and non-metals, *i.e.*, it is a metalloid and is used commonly in semiconductors.[106] Even then, due to its electron deficiency along with multicenter bonds,[32,76,77] boron is gifted with some interestingly unique desirable properties when it is in its 2-dimensional form, *i.e.*, as borophene. Among the borophene allotropes, 2-*Pmmn*, χ^3 and β_{12} phases include properties like mechanical flexibility, metallicity, transparency, superconductivity, selectivity, sensitivity, *etc.*

4.1. Mechanical properties

The scientific research communities have shown great interest in the mechanical properties of borophene due to its mechanical modulus with ultrahigh value, strong B–B bonds and uniqueness in atomic structures[107–109] and have described that chemical modification, number of layers, temperature and the vacancy defects of borophene also contribute to their unique mechanical properties,[110] and its mechanical strength can be determined by a few of the interpretative parameters including lateral size, anisotropy, reduced dimensionality, and disparate polymorphs.

For studying the chemical modulation effect, researchers have been performing physical and theoretical experiments on different borophene forms to find their mechanical coefficients.[111] Nonetheless, few results have disclosed that there is a decrease in the coefficients of different forms of borophene due to electrochemical fluorination. It has been reported that after the fluorination of 2-*Pmmn* borophene, two anisotropic structures B_2F and B_4F,[112] with high stability were obtained, which showed good thermal, electrical and mechanical conductivity properties and were thus identified as encouraging candidates for electronic devices as semiconductors.[106] Similarly, on hydrogenation of borophene (borophane), the Young's modulus of 2-*Pmmn* phase along its zigzag and armchair directions decreased to 110.59 and 172.24 N m^{-1}, respectively, indicating an increment in mechanical flexibility.[111] The reason for the decrease in Young's modulus was investigated and it was proved that on hydrogenation the B–B bonds become elongated from 1.616 Å to 1.941 Å, leading to the bond strength decrement, which reduces Young's modulus. Moreover, critical strain increased along all three directions (zigzag, armchair and biaxial) after the hydrogenation (a comparison of borophane

Open Access Article. Published on 21 April 2022. Downloaded on 2/8/2026 10:57:22 PM.
This article is licensed under a Creative Commons Attribution-NonCommercial 3.0 Unported Licence.

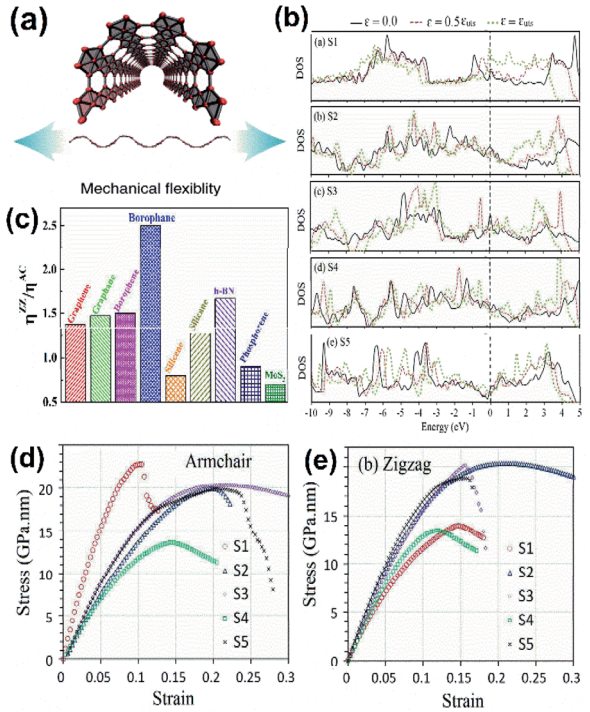

Fig. 14 (a) Diagram showing the mechanical flexibility of borophene. (Reproduced from ref. 105 with permission from Elsevier). (b) Comparison of the electronic DOS for the densest borophene (S1) and borophene with an increase in vacancy defect concentration (S2–S5) across the armchair direction with respect to different strains (ε) and at maximum tensile strength (ε_{uts}). (c) The ratio of overall strain in the zigzag (η_{ZZ}) and armchair (η_{AC}) directions for different 2D materials. (Reproduced from ref. 111 with the permission of the Royal Society of Chemistry). (d and e) Variation in Young's modulus across the (d) armchair direction and (e) zigzag direction with an increase in the conc. of vacancies from (S1–S5). (Reproduced from ref. 108 with the permission of the Royal Society of Chemistry).

with other 2D material is shown in Fig. 14(c)),[50,111] which maintained its stability until the tensile uni-axial strain along the zigzag and armchair directions was up to 22% and 17%, respectively.[113] Later, the analysis of α_1-borophene and γ-B_{28} (ref. 92 and 114) showed that boron sheets are able to open a new bandgap after hydrogenation, which can act as a semi-conducting material.

The study of multi-layer borophene of the 2-*Pmmn* phase was able to relate the variation in the mechanical properties due to the effect of change in the number of layers, wherein Young's modulus was measured as 136 N m^{-1}, 141 N m^{-1}, 144 N m^{-1}, 158 N m^{-1} along the zigzag direction, and along the armchair direction it was 338 N m^{-1}, 360 N m^{-1}, 380 N m^{-1}, 397 N m^{-1} on varying from a four-layered borophene to a monolayered one, respectively, revealing that Young's modulus is maximum for the one with four layers. Hence, borophene exhibits superior mechanical properties similar to black phosphorene on increasing their layers.[115] A monolayered borophene is extremely flexible and is indicated as a promising nanomaterial for wearable devices.[53]

It was found that when boron concentration was 4/27th of the total borophene concentration, along the zigzag direction, Young's modulus reduced from 180 N m^{-1} to 87 N m^{-1} when the temperature was increased from 1 K to 600 K, indicating the inverse proportionality of Young's modulus with temperature.[115]

The results of mechanical properties seen in Fig. 14(d and e) revealed the inverse proportionality of Young's modulus to vacancy defect along the armchair direction, and Fig. 14(b) revealed the inverse proportionality of borophene density of states to vacancy defect concentration, which also decreased its tensile strength.[108] Borophene with phase β_{12} and χ^3 had a much smaller Young's modulus when compared to the 2-*Pmmn* phase across the armchair direction, whereas along the zigzag direction, Young's modulus was not much affected by the vacancy defects. Along with this, it was observed that for α sheet, β_{12} and χ^3, the critical strains across both in-plane directions were much larger when compared to the defect-less 2-*Pmmn* phase borophene. Nevertheless, the atomic displacement method indicates that an increase in hollow hexagons reduces B–B bonds, causes a stiffness change in borophene, and increases the hardness of the material, indicating the effect of hollow hexagons on its mechanical strength.[31,67]

4.2. Chemical properties

Focussing mainly on the reactivity of borophene during the chemical reaction, *i.e.*, metallicity, boron ([He]2s^{2}2p^1) located between carbon (nonmetallic) and beryllium (metallic), exhibits both metallicity and non-metallicity due to the presence of 2p electrons along with orbit radius near the 2s state.[41,116] One of its interesting facts is that its 2-dimensional structure shows intrinsically high anisotropic metallic properties[7] and few of its allotropes with Dirac fermions are also semi-metallic.[39] Along with allotropes 2-*Pmmn*, χ^3 and β_{12}, the honeycomb borophene phase also exhibits metallic behavior,[117] diverging from its triangular and hexagonal lattice structures.[30] These metallic characteristics were predicted theoretically by Zhang *et al.*[81] and experimentally confirmed through the STM data.[15] The theoretical results[118] in which the two bands crossing the Fermi energy as in Fig. 15(c) and the dispersion of the Fermi surfaces $E_F = E^{BS}(k_x,k_y)$ throughout the Brillouin zone as in Fig. 15(d) are in agreement with the previous studies,[61,119] and revealed that borophenes are metallic. When compared with the spin–orbit couplings of other 2-D materials and graphene, borophene has a negligible spin–orbit coupling and is considered the lightest 2D material showing metallic properties in which there was linear dependence of energy on momentum, *i.e.*, a Dirac metallic material.[120]

Based on the PBE functional, DOS corresponding to the band structure of α_1-2H borophene indicated in Fig. 15(b) proved its metallicity recently, which was in agreement with the UV-visible and PL results.[98] Further, a distinct metallic property was observed when borophene formed a heterostructure with any other 2D materials.[32]

By the technique of thermal decomposition, a newly introduced borophene on Ir(111) also showed metallic character as specified by the results of the dI/dV curve in Fig. 15(eand f), where the decrement in the Fermi level to form a V-shape is

© 2022 The Author(s). Published by the Royal Society of Chemistry

Open Access Article. Published on 21 April 2022. Downloaded on 2/8/2026 10:57:22 PM.
This article is licensed under a Creative Commons Attribution-NonCommercial 3.0 Unported Licence.

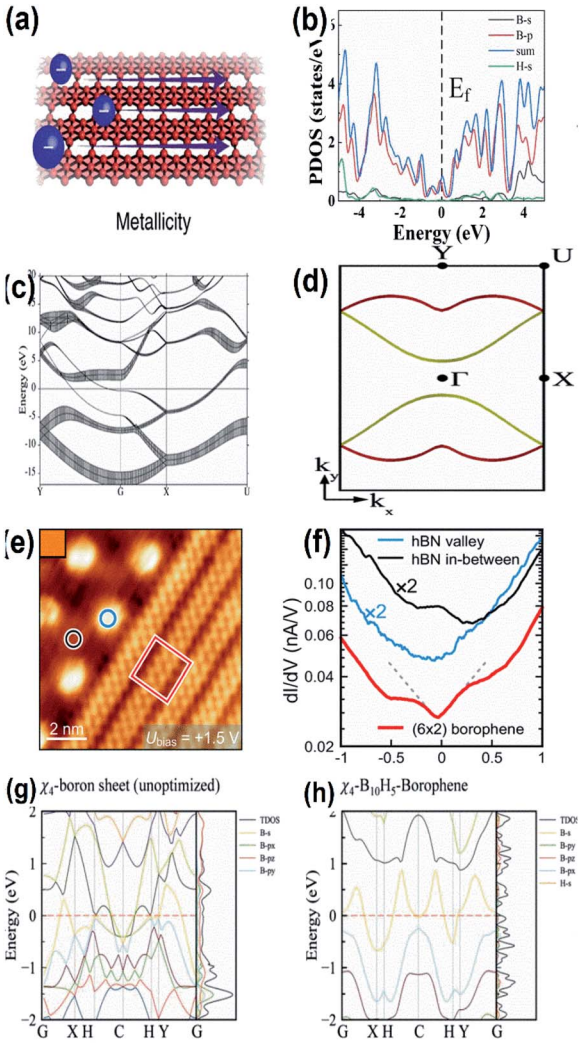

Fig. 15 (a) Diagram showing the metallicity of borophene, (reproduced from ref. 105 with permission from Elsevier). (b) DOS with electronic band structure for α_1-2H borophene with different colours for different orbitals of borophene (where blue: total DOS, black: B-s, red: B-p, green: H-s) with respect to the valence band maximum. (Reprinted with permission from ref. 98. Copyright (2021) American Chemical Society). (c) Band structures for the sheets of borophene plotted along high symmetry points; fat bands indicate the sp character of the σ-bond, where the Fermi energy lies at $E = 0$ and the Γ point is represented by G. (d) The 2-dimensional Fermi surface of the electronic energy (EE) bands crossing the Fermi energy in (c) is represented in red and yellow. (Reprinted with permission from ref. 118, Copyright (2019–2020) American Physical Society). (e) STM image of (blue circle) valley hexagonal boron nitride, (black circle) mesa hexagonal boron nitride, (red square) borophene. (f) d*I*/d*V* spectra representing the images marked in (e) in their respective colours. (Reprinted with permission from ref. 99 Copyright (2021) American Chemical society). (g, h) Band spectrum including TDOS and PDOS of χ^4-borophene with (g) no hydrogen atom and (h) 5 hydrogen atoms. (Reprinted with permission from ref. 121, Copyright (2021) American Chemical Society).

partial evidence for borophene on Ir(111) showing the Dirac-like behavior.[99] The presumed electronic band structures of χ^4-5H-borophene indicated in Fig. 15(g and h), disclosed its metallic behavior based on the Density Functional Theory (DFT) through the Vienna *ab initio* Simulation Pack (VASP),[121] where the metallic behavior is significantly contributed by the p-orbitals, which is comparable to previous reports[122] indicating χ^4-5H-borophene to be suitable for employment in the applications of memory devices as well. Moreover, the same can also be identified by the 3 bands (2 in the G–X direction and 1 in the S–Y direction) in the Fermi level.[7] The metallic structure of a single-layered borophene was due to the overlapping of their electronic bands at the Fermi level[45] in which the metallic states were predicted to originate due to the appearance of the band gap near the Fermi level as a result of their corresponding $2p_x$ and $2p_y$ states.[54]

Chemical modifications like hydrogenation, fluorination, and lithiation can also affect the metallic properties.[110] On hydrogenation, the band structure of the 2-*Pmmn* phase changes to that of a semiconductor with zero bandgap and even in a state free of stress, a metallic band structure is observed in graphene-like borophene, and a biaxial or uniaxial shear strain can cause the transition of the metallic band structure to a semiconducting one (Fig. 16(a–c)).[123] The theoretical results of fluorinated borophene were investigated and the energy band structure as shown in Fig. 16(d–f) revealed that B_4F is metallic and B_2F is an indirect semiconductor.[112] Metallic characteristics were exhibited by the electronic structures during the lithiation process,[124] indicating that borophene is an excellent electronic conductor with high ionic conductivity. Moreover, the β_{12} and χ^3 phases when used as an anchoring material in Li–S batteries showed electronic structures with metallic properties during their entire discharging and charging cycles.[110] As predicted previously, even the PDOS of the borophene heterostructure with Li proved that the lithiation process does not diminish the metallicity of the entire system completely (Fig. 16(g and h)),[125] whereas the interactions of halogen atoms or molecules with borophene, do not alter its metallicity.[126]

These metallic features of borophene are useful for the sensing of various small molecules and gases although it depends primarily on the electronic structure.[127] Since metallic borophene consists of abundant electrons, it can be used for catalysis as well.[128] It has been predicted that even the conventional superconductivity mediated by phonon is due to the intrinsic metallicity.[32]

4.3. Electrochemical properties

Electrochemical properties are among the most essential for various applications such as energy storage and sensing, and researchers are still finding ways to improve the electrochemical properties of existing nanomaterials that are already used as sensors, as well as finding new efficient materials for the same. The atomic configuration is one of the important parameters that has opened up platforms for the development of sensors and interestingly, in the case of borophene, rather than the usual binding, the existence of additional electron-deficient bonds inspires it towards the sensing properties.[3] However, the comparatively low conductance of borophene identified during the previous reports on their electronic properties[5] is one of the main motives for sensing hydrogen coverage.

Open Access Article. Published on 21 April 2022. Downloaded on 2/8/2026 10:57:22 PM.
This article is licensed under a Creative Commons Attribution-NonCommercial 3.0 Unported Licence.

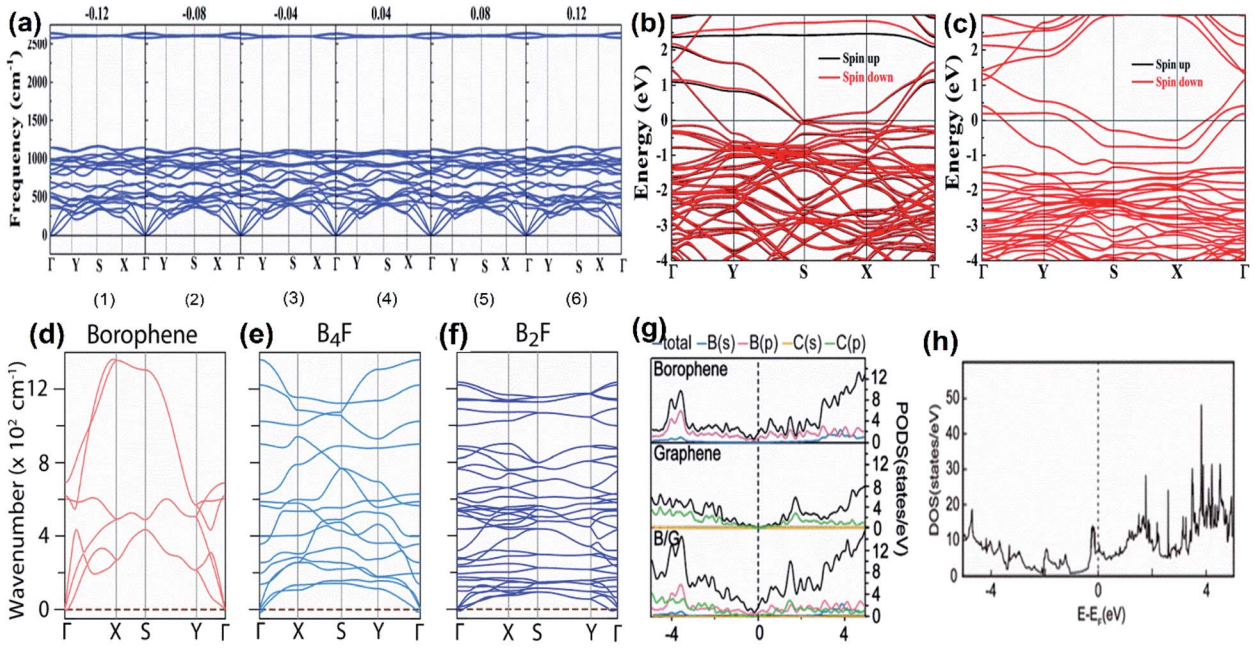

Fig. 16 (a) Dispersion of phonon for W-borophane (completely hydrogenated borophene) under different shear strains. (b–f) Electronic band structures of W-borophane: (b) with H vacancy, (c) with a dimer (B–H) vacancy. (Reproduced from ref. 123, published by Royal Society of Chemistry licensed under Creative Common Attribution Non-Commercial 3.0 Unsupported license). (d) Pure borophene, (e) B_4F, (f) B_2F, (reproduced from ref. 112, published by ACS Author Choice). (g) Total and partial DOS of borophene, graphene, borophene/graphene. (h) Total DOS of B/G with single Li (reprinted (adapted) with permission from ref. 125. Copyright (2020) American Chemical Society).

Moreover, electron mobility along with metallic structure is necessary for exhibiting various sensing properties including photonic, electronic, thermoelectric and thermal sensing for numerous small molecules and gases.[129] The adsorption of ammonia[130] and HCN[105,131] is one of the parameters that suggests that B_{36} can sense ammonia and HCN; there was a variation in the electronic properties at the B_{36} edges when compared to its other configurations.[105] Recently Wu *et al.*[98] reported the photosensitive properties of PMMA-supported borophene through the results of photocurrent *versus* reverse bias on varying the light power (Fig. 17(b)).[98] The Fe_3O_4 nanoparticles, when functionalized by borophene to result in χ^4-borophene, exhibited good sensing properties due to the core–shell structure.[121] Ultrasensitive molecular sensing could be delivered by borophene due to its ridgelines (an excellent molecule anchor) along with light and strain sensitivity.[103]

Although there are rare reports on the sensing property of substrate-supported borophene, the first synthesized independent borophene sheets by Ranjan *et al.*[93] showed its ability to sense the gas, strain and molecules based on the surface-enhanced Raman spectroscopy (SERS). Even though both β_{12} and χ^3 phases of borophene exhibited metallic behavior, only the β_{12} phase has the ability to sense the molecules with the help of electrical signals due to the increment in the mobility of electrons along the ridgelines.[132]

Firstly, the sensing property of borophene was identified by the first-principles calculations.[105] Theoretical analysis through DFT calculations have indicated the suitability of borophene particularly for the toxic gas sensing wherein the adsorption of NH_3, NO_2, CO_2, NO and CO gas molecules was observed by analyzing the transport and electronic properties of borophene sheets within the Perdew–Burke–Ernzerhof exchange-correlation functional and generalized gradient approximation using VASP27, and it was observed that the binding energy was low for CO_2 molecules and high for the remaining gases.[133] The theoretical results using the Cambridge Sequential Total Energy Package (CASTEP) also revealed that borophene could be an actively good material for the sensing of CO_2 molecules.[134] Similarly, the adsorption of NO, H_2, N_2, O_2, H_2O, CO and NO on B_{36} sheet revealed by the DFT results indicated that B_{36} can detect NO, CO and O_2.[131] The employment of the Minnesota 06 and B97D functionals using DFT predicted the increase in the electrical conductivity in the presence of formaldehyde, which indicated that B_{36} exhibited the property of sensing formaldehyde.[135] Furthermore, there have been findings of borophene with electronic and energetic sensitivities for nucleobases (adenine, cytosine, guanine and thymine).[136]

Borophene is highly sensitive for the detection and transmission of electronic signals.[135] The sensitivity of borophene can be further enhanced for transforming stimuli such as pH and temperature into mechanical, optical and electrical signals when combined with hydrogel-based substrates.[81] Lherbier *et al.*[137] proved the improvement in the photosensitivity of borophene through its surface modifications. Also, their high surface volume ratio is one of the favorable properties for detecting gas molecules with low concentration. As observed from the results of *I–V* characteristic data as shown in Fig. 17(c and d), borophene showed the variation in its electrical

© 2022 The Author(s). Published by the Royal Society of Chemistry

Open Access Article. Published on 21 April 2022. Downloaded on 2/8/2026 10:57:22 PM.
This article is licensed under a Creative Commons Attribution-NonCommercial 3.0 Unported Licence.

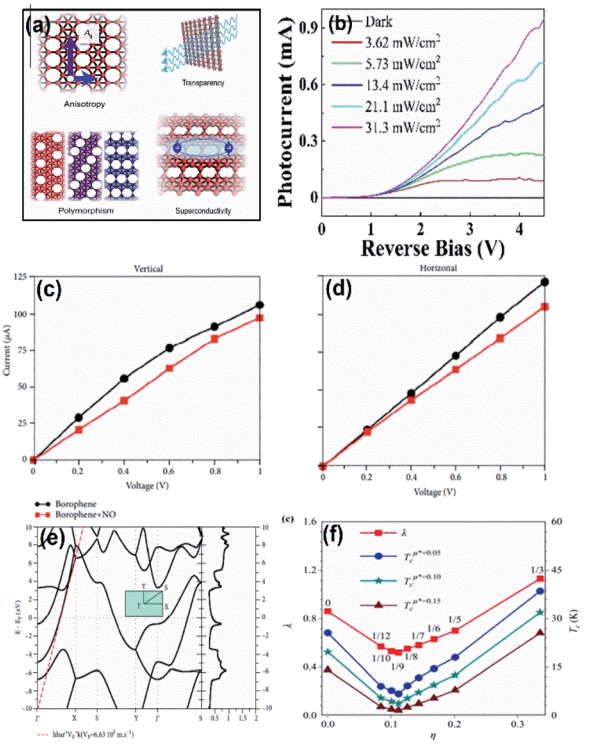

Fig. 17 (a) Diagram indicating the anisotropic and polymorphous structure of borophene favoring its properties like transparency and superconductivity. (Reproduced from ref. 105 with permission from Elsevier). (b) Variation in the photocurrent *vs.* reverse bias on PMMA-supported borophene (reprinted (adapted) with permission from ref. 98. Copyright (2021) American Chemical Society). (c) Vertical and (d) horizontal variations in *I*–*V* curves for bare borophene (black) and on addition of NO (red). (Reprinted (adapted) with permission from ref. 138. Copyright (2018) American Chemical Society). (e) Band structures and DOS with Fermi-energy aligned initial energy. (Reproduced from ref. 137 with the permission of IOP Publishing Ltd.). (f) Graph of wavelength (λ) and transition temperature (T_c) *vs.* the vacancy concentration of boron (η). (Reproduced from ref. 70 with permission from AIP Publishing).

properties with the addition of NO; the decrease in band gap and change in the adsorption energy when treated with ethanol also indicated the sensitivity of borophene for ethanol vapor.[138] Further, the property of gas adsorption for spintronic and gas sensor devices could be improved by embedding borophene with the atoms of transition metals.[139] Hence, the outstanding sensing properties of borophene has helped it to emerge in various fields.

4.4. Electrical properties

Borophene with a combination of high electrical, ionic, optical and thermal conductivities serves as an outstanding material for various applications.[110] Herein, we mainly focus on its electrical and thermal conductivity. For borophene with the 2-*Pmmn* phase, the electrical conductivity is higher along the armchair direction when compared to that of the zigzag direction.[123] Studies on the electron–electron and electron–phonon interactions by state-of-the-art methods showed that electrical conductivity is controlled by electron–phonon interactions[38] and as seen in Fig. 17(e), an important role is played by the Fermi velocity for the electrical conductivity when the electron–phonon relaxation time is closer to the Fermi level (EF) and the density of states is at EF.[137] Moreover, the conduction of electricity is facilitated by the construction of metallic bands in borophene. Along with this, the tendency of borophene to donate electrons motivated the research on halogen atom (F, Cl, Br, I) interactions with borophene, and on analyzing the single halogen migration on borophene surface it was observed that high diffusion barriers which decrease with atomic size were able to alter the anisotropy of electrical conductivity.[126] The electrical conductivity of the electrode can be further improved when Li/Na atoms are absorbed by borophene, showing its metallic property, which has low open-circuit voltage when treated as the anode material[105] and especially during the complete lithiation process the electrical conductivity of borophene was excellent due to the metallic characteristics observed in its electronic structure.[124] In a study,[136] the variation in electrical conductivity was also observed when B_{36} borophene was in contact with different nitrogenous bases. The boron vacancy and good electronic conductivity of borophene highlight its ultrahigh ionic-conductivity at its 2-*Pmmn* phase representing its best performance during it discharging and charging cycles.[124]

The thermal conductivity of borophene was reported to be much low due to its anisotropy when compare to other similar isotropic 2-dimensional materials.[45] The results of borophene grown on Ag(111) showed low thermal conductivity at its lattice, which was strongly anisotropic as the phonon–phonon scattering was very strong and could be further reduced when the length of the lattice was reduced below 300–400 nm.[140] Using DFT, on solving the Boltzmann distribution for phonon frequency, the thermal conductivity of δ_4 borophene after intercalating it with Al was studied and it was found that thermal conductivity increased along the armchair as well as in the zigzag direction, even though the atomic density of intercalated borophene was large. This was because of the grouping of the acoustic branches in borophene after the intercalation, which decreased the phase space of the phonon scattering process. Along with this, even the anisotropy also got tuned.[141] Mortazavi *et al.*[142] calculated the thermal conductivity through the molecular dynamics at non-equilibrium and observed the effects of strain, where the thermal conductivity of borophene increased largely when strained along the armchair direction, *i.e.*, 250% increment and the increase in thermal conductivity was much less when strained along the zigzag direction, *i.e.*, a 20% increment for a strain of 8%.[142]

Recent investigations on the diffusion property of lithium in the heterostructure of borophene/graphene revealed that the overall conductivity of borophene could be further enhanced through the borophene/graphene heterostructure.[125] The study of the optoelectronic properties of δ_6 and β_{12} *via* the perturbation theory and DFT revealed that both allotropes of 2D boron are optically transparent, which strongly depends on the energy and thickness; a weak absorbance was also observed in the

Open Access Article. Published on 21 April 2022. Downloaded on 2/8/2026 10:57:22 PM. This article is licensed under a Creative Commons Attribution-NonCommercial 3.0 Unported Licence.

visible range. This also introduced borophene as a good material for nano-optoelectronics with tunable monolayers.

4.5. Magnetic properties

Various 2-dimensional materials, especially Dirac materials, are being investigated based on their superconductivity behavior[143] and it was reported that graphene becomes superconducting when heavier atoms are doped into it.[144] Similarly, borophene being another 2D Dirac material is also reported to show superconductivity properties[79,116,145,146] due to its low mass along with a powerful electron–phonon coupling. The hexagonal molecular geometry with different critical temperatures favors the superconducting properties of borophene.[116] Since the electronic states of the Fermi surface are occupied by both σ and π electrons of borophene, it shows superconductivity. Through analysis of the phonon spectra, electron–phonon coupling and electronic structure, borophenes are reported to disclose phonon-mediated superconductivity at the transition temperature $T_c \sim$ 10–20 K.[72] As indicated in Fig. 17(f), a systematic study on the dependence of T_c on the density of hexagonal holes showed a V-shaped curve, where T_c is inversely proportional to the vacancy concentration up to $x = 1/9$ and later becomes directly proportional, which can be observed in bilayer borophene intercalated with transition metals. It even proved that T_c is high when DOS is large at the Fermi surface.[70] For the free-standing 2-*Pmmn* phase, T_c was 19 K due to powerful electron–phonon coupling as a result of the solid Fermi surface and high DOS at the Fermi surface.[147] Other substrate-supported phases of borophene including β_{12} and χ^3 also exhibited superconductivity with a transition temperature of 14 K and 12 K, respectively.[145] Additionally, bilayer borophene intercalated with Mg (BxMgBx), *i.e.*, the Mg–B system, also displayed excellent superconductivity with $T_c = 23.2$ K and 13.3 K, respectively, for $x = 2$ and 4.[116]

The superconductivity can be further tuned for free-standing, substrate-supported, and bilayer metal-intercalated borophene. The T_c of 2-*Pmmn* borophene can be altered either by the strain or doping carriers, and the in-plane orbital density states close to the Fermi surface relate their impact on T_c, where tensile strain and the doping of holes increases T_c, *i.e.*, T_c of the 2-*Pmmn* phase increased to 27.4 K and 34.8 K, respectively, while compressive strain and the doping of electrons decreased T_c.[147] However, there was a reduction in T_c to 0.09 K when 0.1e of electrons was doped per boron in the β_{12} phase.[145] Moreover, the superconductivity for borophene supported by a substrate can also be probed experimentally by inducing suppression through electron doping and with the decrease in the in-plane projected DOS at the Fermi-level, the T_c for the Mg–B substrate also decreased. This superconductivity can also be closely related to the intrinsic structure of the crystal.[27]

5. Stability of the different isomers of borophene

With an increase in the concentration of vacancies in the 2D allotrope of boron, the evolution of the triangular lattice structure into a hexagonal lattice[72] is the fundamental principle behind the extensive findings of 4239 isomers of borophene.[68,72] These isomers include both categories of borophenes, *i.e.*, those with hexagonal holes (HHs), as well as with large holes (LHs). However, with stability being an important aspect in experimental synthesis along with production on a large scale, numerous theoretical studies have been proposed in which the high stability in the planar sheets of boron is reported due to the presence of vacancies.[97] It has been reported that borophene isomers with LHs have high stability at higher vacancy concentrations and slightly lower stability at lower vacancy concentrations when compared to the isomers with only HHs.[148] Few of the theoretical studies reported B_{36} with a quasi-planar cluster of borophene to have high stability;[50] there were also predictions on the stabilities of *Pmmm*, *Pmmn*, struc-1/8-, snub-, $g_{1/8}$-, $g_{2/15}$-, α_1- and β_1-sheets.[39,68,72,74,149] Further, to study the crystal structure stability in detail, it can be differentiated as dynamical stability, thermodynamical stability and mechanical stability.[97]

5.1. Dynamical stability

Two parallel experimental studies reported the successful growth of borophene on a substrate of Ag, which mainly proposed three structures, *i.e.*, stripped borophene, χ^3 and β_{12}.[15,45] The dynamic stabilities of different phases of borophene were studied.[74] Any crystal structure is said to be dynamically stable when the imaginary frequencies of phonons are absent.[150] In Fig. 18(a–c), the absence of imaginary vibration modes for χ^3 and β_{12} indicates their kinetic stability at 0 K. However, striped borophene is dynamically unstable, since the frequency of vibration of striped borophene becomes imaginary along the direction of -X at the longer wavelength limit.[7,45] In support of this, a theoretical study showed the dynamic instability of free-standing striped borophene even when the tensile stress was very high.[31]

5.2. Thermodynamic stability

Phonons determine the relative stability of the crystal structure at 0 K as well as finite temperature *via* Helmholtz free energy, describing their thermodynamical stability.[150] The Helmholtz free energies of stripped borophene, χ^3 and β_{12} after including the zero-point energy at 0 K were found to be −6.106, −6.159, −6.145 eV per atom, respectively. These values were altered at higher temperatures, as shown in Fig. 18(d), for an increase in temperature between 0 K and 1000 K. Helmholtz free energy is in the order $\chi^3 < \beta_{12} <$ stripped borophene, which indicates that for a wide range of temperatures, χ^3 and β_{12} are thermodynamically very stable when compared to stripped borophene.[97]

5.3. Mechanical stability

The fulfillment of the Born–Huang criteria is essential to confirm the mechanical stability; the observed elastic constants for all three phases of borophene satisfy the criteria for Born stability,[97] indicating their mechanical stability. Nevertheless, through Fig. 18(e and f), Young's modulus and Poisson's ratio were compared with the other 2D materials and it was found

 © 2022 The Author(s). Published by the Royal Society of Chemistry

Open Access Article. Published on 21 April 2022. Downloaded on 2/8/2026 10:57:22 PM.
This article is licensed under a Creative Commons Attribution-NonCommercial 3.0 Unported Licence.

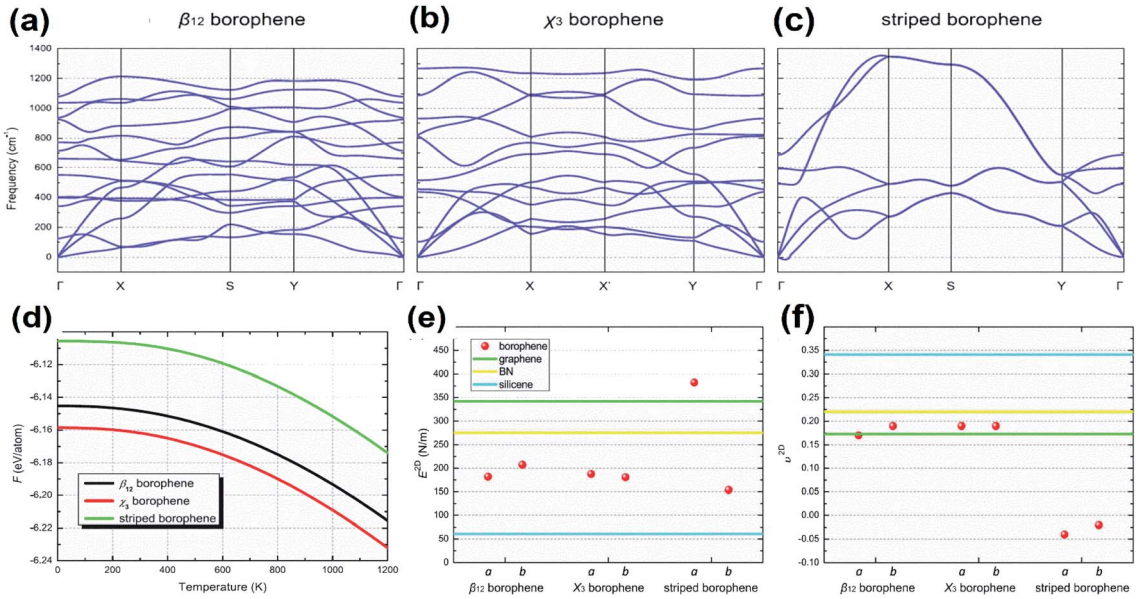

Fig. 18 (a–c) Dispersion of phonons with different lines of symmetry for the (a) β_{12} phase, (b) χ^3 phase, (c) striped borophene. (d) Helmholtz free energy varying with the increase in temperature for the β_{12} phase (black), χ^3 phase (red), striped borophene (green). Comparison of (e) Young's modulus and (f) Poisson's ratio for all three phases of borophene (red dots), graphene (green line), boron nitrate (yellow line), silicene (blue line). (Reproduced from ref. 97, published by Taylor & Francis Group, licensed under Creative Common Attribution.)

that the stiffness of χ^3 and β_{12} was lower than in BN and graphene but higher than in silicene.[151]

Furthermore, updated research on the mono- and double-doping of carbon atoms into β_{12}, related to the resulting decrease in π-electrons, increase in σ-electrons and decrease in coordinated atoms from 4 to 6 in the double doped β_{12}, contributed to a much better understanding of the stability.[152]

6. Advantages over graphene

After the synthesis of borophene, researchers have been characterizing the properties of borophene in order to find its advantages as compared to graphene and other 2-dimensional materials, and have found that borophene is stronger, more flexible, a good conductor of heat and electricity and a superconductor when compared to graphene; all these properties can also be tuned depending on the arrangement as well as the orientation of vacancies in borophene.[97] Moreover, the electron-deficient behavior of boron causes the formation of borophene with multicenter bonds possessing several desirable unique physical properties.[108] A much lighter, electron-rich borophene is also estimated to be an equivalent competitor of graphene due to its remarkable mechanical properties[45] along with orientationally controllable properties for various applications.

A theoretical analysis demonstrated that borophene with a hollow hexagon concentration of 1/6 has a bending stiffness that is twice that of graphene and even though the H–H bonds are absent in the boron sheets, they are much stronger than graphene, which makes borophene a better replacement for advancement in the composites.[67] In the armchair direction, borophene with the phase *Pmmm* and 2-*Pmmn* has a much larger Young's modulus (574.61 N m^{-1} and 398 N m^{-1}) when compared to that of graphene (338.08 N m^{-1}),[110] which highlights the interesting mechanical properties of borophene over graphene. Strikingly, although the interaction of H_2 with borophene is similar to that of graphene, its capacity for hydrogen storage is greater than the capacity of graphene[153–155] and the binding energies of gas molecules such as NO_2, NO, CO_2, NH_3 and CO are also stronger on borophene when compared to the reports on other 2D material.[156,157] Hence, borophenes are highly recommended for the detection of toxic gases, as other 2D materials including graphene lack high selectivity and sensitivity due to their zero-band gap.[3]

Interestingly, theoretical calculations revealed that metallic borophene sheets with an exceptional anisotropic behavior[74,158] are a better conductor of electricity[38,159] and possess better properties for thermal transport[140] when compared to graphene. Moreover, the stability induced by the substrate on borophene frames an intermediate class of covalently bonded, templated sheets having distinct properties along with consistent structures when compared to other previously reported 2D materials.[160]

7. An interesting material for numerous applications

Presently, borophene is considered to be a potential material for a range of applications in various fields. Physicists are entranced by the ability of borophene as a sensor for the detection of various kinds of molecules and their atoms.[133,161–164] Chemists are excited about its catalytic capability,[152,165–170] and electrochemists are researching borophene as a good anode

Open Access Article. Published on 21 April 2022. Downloaded on 2/8/2026 10:57:22 PM. This article is licensed under a Creative Commons Attribution-NonCommercial 3.0 Unported Licence.

material for the generation of a better, powerful metal-ion battery.[4,125,171–173] Borophene also exhibits potential in various other applications.[5,38,106,174–178]

7.1. Biomedical applications

Borophene as a 2D nanomaterial has attracted significant attention and has been studied widely in the field of biomedicine because of its good flexibility.[53] It can be considered one of the promising biomaterials since it shows different physical and chemical characteristics in its different phases, which could be heterogeneously personalized for various biomedicines as well as medical devices.[106] The unstable nature of honeycomb borophene satisfies the biodegradability essential for biomedical applications.[53] When combined with metals and semiconductors, borophene showed improvement in the biological applications without negative impacts.[50]

Recent reports indicated that the sequencing of DNA is done in different ways by determining the sequence of the base, which is essential for decoding the human biological code,[179,180] and several studies regarding medicine and biology have been conducted.[181,182] The results of the electron sensitivity of B_{36} borophene towards 4 nitrogenous bases, cytosine (C), thymine (T), guanine (G) and adenine (A), over DNA showed that borophene when attached to different bases as shown in Fig. 19(a) gave different electrical signals and conductivity, as well as variations in energy and energy gap as shown in Table 2, provoking it to be used in devices for the sequencing of DNA.[136]

Tumor therapy is one of the fields that has popularized nanomaterials because tumors exhibit enhanced permeability and retention (EPR) effect; drugs with sizes of 10 to 1000 nm can enrich the tumor site to passively target tumors, reduce side effects and improve efficacy.[183,184] Additionally, drug delivery is more advantageous through borophene as it can make itself stable by easily combining with other groups or elements. Nonetheless, drug delivery often requires special group modification to stabilize the delivery system of the body and for the accurate release of the drug at the tumor site.[185,186] As indicated in Fig. 19(b and c) the fluorescence image of the malignant tumor could be identified by easily differentiating it from that of normal tissue in the case of a tumor mouse injected with PEG-modified Cy5.5 borophene (B-PEG/Cy5.5NSs) when compared to the tumor mouse injected with bare Cy5.5.[88] This promotes the application of borophene towards bioimaging, which includes photothermal imaging, photoacoustic imaging and fluorescence imaging.[21]

Cancer treatments can be achieved with minimal invasiveness through photothermal therapy, where NIR radiation is used to irradiate the tumor, which kills the tumor cells by increasing their temperature by photothermal conversion.[187] A better therapeutic effect was observed in the case of borophene due to its UV absorbance property, and efficacy in photothermal conversion and photothermal stability; hence borophene was a potential candidate for photothermal tumor therapy.[88] Furthermore, biomedical performances such as biocompatibility, targeting ability, circulation, and loading capacity can be enhanced by the appropriate functionalization or surface modification. Surface-functionalized Xenes when compared to their pristine form showed enhanced surface reactivity, stability of dispersion and invoked degradation kinetics, which minimized the toxic response and maximized the biological outcomes.[188] Hence, the exfoliation of borophene after modification by PEG-NH_2 (molecular weight = 2000) by powerful electrostatic adsorption, reported a layer with about 33.6% (w/

Table 2 E_{ad} (adsorption energy in kcal mol^{-1}), E_{HOMO} (HOMO energy), E_{LUMO} (LUMO energy), E_g (energy gap of the HOMO and LUMO) in eV for different complexes formed by B_{36} (Fig. 22) when combined with different nucleobases, and ΔE_g represents the change in the energy gap after the adsorption. (Reproduced from ref. 136 with the permission of Elsevier)

System	E_{ad}	E_{HOMO}	E_{LUMO}	E_g	ΔE_g (%)
B_{36}	—	−5.05	−4.01	1.04	—
Adenine/B_{36}-1	−19.7	−4.89	−3.91	1.06	+1.6
Adenine/B_{36}-2	−39.2	−4.37	−3.52	0.86	−17.5
Adenine/B_{36}-3	−57.3	−4.38	−3.51	0.87	−16.3
Adenine/B_{36}-4	−45.5	−4.43	−3.60	0.83	−20.2
Cytosine/B_{36}-1	−38.1	−4.19	−3.49	0.71	−32.0
Cytosine/B_{36}-2	−4.8	−3.81	−3.77	0.05	−95.5
Cytosine/B_{36}-3	−34.7	−4.00	−3.69	0.30	−70.9
Guanine/B_{36}-1	−35.2	−4.45	−3.58	0.88	−15.3
Guanine/B_{36}-2	−43.1	−4.67	−3.80	0.88	−15.6
Guanine-3	−37.3	−4.04	−3.15	0.88	−14.8
Guanine-4	−22.3	−3.98	−3.43	0.54	−47.9
Guanine-5	−20.5	−4.15	−3.39	0.76	−26.6
Thymine-1	4.4	−4.31	−3.57	0.74	28.9
Thymine-2	10.2	−4.27	−3.60	0.67	−35.5

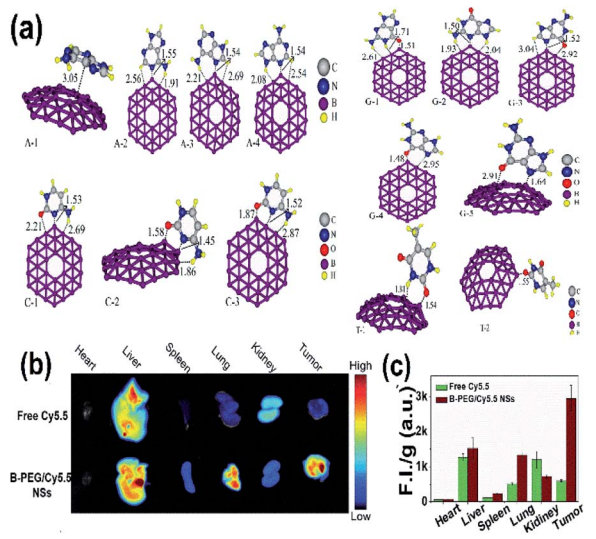

Fig. 19 (a) Different nucleobase/B_{36} complexes {adenine/B_{36} (A-1, A-2, A-3, A-4), cytosine/B_{36} (C-1, C-2, C-3), thymine/B_{36} (T-1, T-2), guanine/B_{36} (G-1, G-2, G-3, G-4, G-5)} consisting of carbon (white), nitrogen (blue), oxygen (red), boron (purple), hydrogen (yellow) formed after optimization. (Reproduced from ref. 136 with the permission of Elsevier). (b) Fluorescence imaging (FI) of tumors and other organs. (c) Comparison of (FI) for bare Cy5.5 (green) and B-PEG/Cy5.5NSs (brown). (Reproduced from ref. 21, published by Wiley-VCH GmbH, Licensed under Creative Common Attribution 4.0 International).

© 2022 The Author(s). Published by the Royal Society of Chemistry

Open Access Article. Published on 21 April 2022. Downloaded on 2/8/2026 10:57:22 PM.
This article is licensed under a Creative Commons Attribution-NonCommercial 3.0 Unported Licence.

w) of PEG in the resulting material. This could release a better borophene than its bare form with better dispersibility and stability, resulting in agglomeration in the cell culture medium and phosphate buffer saline,[88] which could be a favorable factor for both theragnostic and therapeutic applications.[188]

7.2. Energy storage applications

The energy storage applications include metal-ion batteries, supercapacitors, hydrogen storage devices, solar cells, *etc.* Most frequently, the energy storage capacity of borophene is theoretically investigated through software simulations of molecular dynamics.[176]

7.2.1. Metal-ion batteries. The combination of electrical conductivity with the thermal stability of borophene makes it a favorable material for metal-ion batteries. The applications of the borophene films as a promising anode material for four different metal ion batteries (Li, Na, Mg or Al) were studied with the help of the simulations from the first-principles density functional theory. The investigation was carried out for four different structures of borophene, which predicted exothermic adsorption when the metal-to-substrate ratio was very high and it was not dependent on the type of atom. The flat borophene when used for the storage of Mg atoms resulted in an ultra-high capacity of 2480 mA h g^{-1} and the capacity of 1640 mA h g^{-1} and 2040 mA h g^{-1} was predicted for the storage of Na and Li, respectively (different charging capacities of different structures of borophene (Fig. 20(a)) are given in Table 3). Even higher capacities were predicted to be accessible on increasing the hole density in the structure of flat borophene. The reasonable charge–discharge rates for the batteries were ensured by the predicted diffusion energy barriers of the metal ions on the surface of borophene. All their theoretical results along with the absence of negative voltage in the voltage profile in Fig. 20(b) suggested that all structures of borophene are efficient anode materials for rechargeable ion batteries.[173]

It was observed that the conductivity of the 2-*Pmmn* phase of borophene was very high with an enormous oxidative process, which allows a charge–discharge process without any dispersion of energy, and hence could serve as a better anode material in Li-ion batteries.[105,106] Moreover, the results from the simulations of *ab initio* molecular dynamics revealed that the specific capacitance of lithiated borophene was 4 times higher as compared to the graphite anode and the energy barrier was much lower than that of Ti_3C_2, and phosphorene served as the anode material. This suggests that borophene when used as an anode for Li-ion batteries, boosts power and energy density.[189] However, modifications such as stratification, hydrogenation or doping alter their interactions; *i.e.*, a Li-ion battery hydrogenated borophene shows good performances,[172] whereas the level of the stored energy is impacted in the Li–sulphide (LiS) battery when β_{12} and χ^3 phases are introduced into it. χ^3 modifies the structure of the LiS battery for the absorption of energy to avoid its structure alteration during charge–discharge cycles and the adsorption energies of Li_2Sn on χ^3 are 2.87, 2.53 and 2.67 for $n = 8$, 6 and 4 respectively, indicating it to be suitable material for anchoring over LiS batteries and although

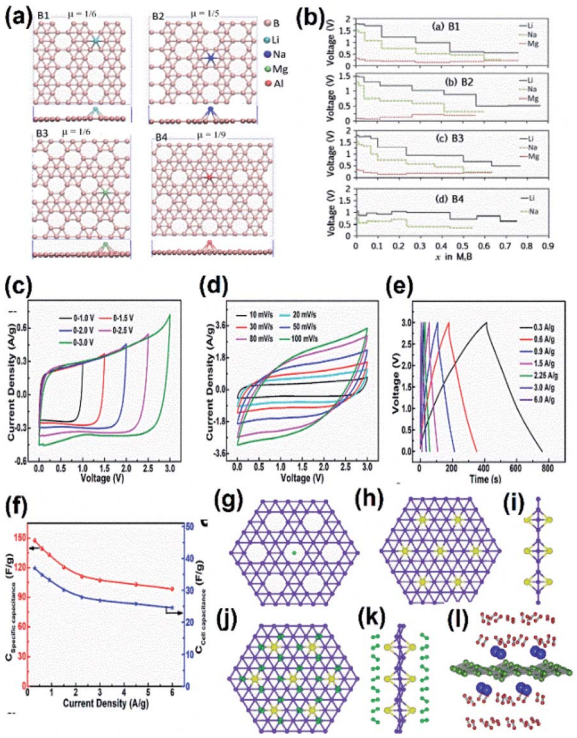

Fig. 20 (a) Top view of borophene sheets with different hole densities (μ) and the metal atoms Li (light blue), Na (dark blue), Mg (green), Al (red) binding their favorable sites to form B_1, B_2, B_3, B_4 respectively. (b) Voltage curve of metal atom coverage for B_1, B_2, B_3, B_4 for its maximum yielding capacity. (Reproduced from ref. 173 with permission from Elsevier). (c–f) Electrolytic properties of borophene supercapacitors. (c) *C–V* results at different voltages. (d) *C–V* results at different scan rates. (e) GCD results. (f) Cell capacitance curve (blue) and specific capacitance curve (red) for varying current densities. (Reprinted (adapted) with permission from ref. 194. Copyright {2018} American Chemical Society). (g) Bare α-sheet borophene. (h) Top view and (i) side view of α-sheet borophene decorated with Li atoms (yellow). (j) Top view and (k) side view of H_2 (green) adsorbed α-sheet borophene decorated with Li atoms (yellow). (Reprint (adapted) with permission from ref. 202. Copyright (2009) American Chemical Society). (l) Side view of the H_2 (green) adsorbed α-sheet borophene decorated with Ca atoms (blue). (Reproduced from ref. 154 with permission from Elsevier).

β_{12} adsorbs just a small amount of energy, it enhances the overall structural stability of LiS. Hence, both defective borophenes enhanced the capacity of retention and suppressed the

Table 3 Charging capacity for the storage of different metal ions when different sheets of borophene are taken as the anode. (Reprinted from ref. 173. Copyright (2017) with permission from Elsevier)

Structure	Hexagonal hole density	Charge capacity (mA h g^{-1})		
		Li	Na	Mg
Buckled	0	1720	1380	1960
B_2	1/5	2040	1480	2400
B_3	1/6	1980	1550	2330
B_1	1/6	1880	1640	2480
B_4	1/9	1840	1340	—

Open Access Article. Published on 21 April 2022. Downloaded on 2/8/2026 10:57:22 PM. This article is licensed under a Creative Commons Attribution-NonCommercial 3.0 Unported Licence.

shuttle effect, which served as excellent anchoring materials for LiS batteries.[87] A LiS battery with high energy density can be realized by stabilizing the polysulphide shuttle and loading high sulphur and this can be achieved when borophene serves as a host for the sulphur cathode, due to its small deformation, high conductivity and strong adsorption.[171]

On considering the sodium-ion battery as an example of ultra-high theoretical capacitance,[189] the potentials of two structures, namely the triangular boron layer (B_{Δ}) and hexagonal vacancies ($B_{\bigcirc}$) were investigated by the first-principles calculations. It was observed that the adsorption energy of Na and specific capacitance for B_{Δ} were −1.731 eV and 248 mA h g^{-1}, respectively, and for $B_{\bigcirc}$ they were −1.448 eV and 298 mA h g^{-1}, respectively. Moreover, the energy barrier for B_{Δ} was just 12 meV, suggesting the extremely fast diffusion and directional anisotropy of sodium in B_{Δ}. Along with this, the metallic characteristics observed during the sodiation process indicate an outstanding electronic conductivity and suggest that it can efficiently serve as an anode for Na-ion batteries, boosting the power density and energy of the batteries.[4]

Due to the small diffusion barrier with high mechanical strength and specific capacity, borophene was predicted to be a potential anode material but it was unstable without a metal substrate. Hence, to improve its stability, researchers recently proposed a new form of borophene establishing van der Waals heterostructures with graphene (B/G), and observed a high absorbance energy (−2.959 eV) and high specific capacitance (1469.35 mA h g^{-1}), with a small specific capacitance (0.613 eV) of Li theoretically increasing the specific capacitance and decreasing the diffusion barrier to 1763 mA h g^{-1} and 0.353 eV, respectively, as a result of the changes made by Li on the distance of interlayers in B/G. This demonstrated B/G to be a new anode material in which its electrochemical performances could be controlled by altering the spacing of the interlayers.[125]

7.2.2. Supercapacitors. Supercapacitors are among the modern energy storage applications with remarkable properties and are of low cost with good charge–discharge rates, which can run for lengthy cycles. The supercapacitor performances are affected by the mechanism of charge storage, surface area and electrical conductivity of the electrode material;[190,191] 2D materials being ultrathin, with wide surface area and high electrical mobility are suitable.[192,193]

Previous studies reported that the supercapacitors consisting of borophene with multi-layers showed good results, *i.e.*, they retained 88% of the initial capacity, even when there was a discharge of more than 6000 cycles[194] it could store a huge amount of energy to serve as a promising biomedical implantable device, especially in rehabilitative robotics.[195] Recent theoretical studies showed that borophene could exhibit better electrochemical performances than graphene, which made it suitable for supercapacitors. The properties include a larger voltage window with high stability (Fig. 20(c)), the CV curves were nearly rectangular even with the scan rate = 100 mV s^{-1} (Fig. 20(d)),[194] and good capacitance behavior with fast charge–discharge rate (Fig. 20(e)). The specific capacitance was 147.6 F g^{-1} for 0.3 A g^{-1} of current density (Fig. 20(f)), and was much higher as compared to bulk boron and carbon-based materials.[196–198]

A very recent study on the capacitive properties through the band structures of eight sheets related to borophene revealed that among them, the Fermi levels of seven sheets consisted of Dirac cones and their carriers had higher velocity than graphene. Hence, the larger differential and integrated quantum capacitance with large charge stored at the surface make them superior electrodes for supercapacitors.[174] The ultrasonic exfoliation of α-borophene and further growth into polyaniline: α borophene through electrostatic repulsion was investigated on a nickel foam substrate and it was reported that its specific capacitance was 960 F g^{-1} and there was 95% retention even after 1000 cycles. This indicated that α-borophene could enhance the performance of polyaniline, making it a promising material for supercapacitors.[175] Thus, all the above results with remarkable features made the supercapacitance of the already existing supercapacitor more advanced when treated with borophene.

7.2.3. Hydrogen energy storage. Considering the environmental issues and finite fuel sources, the development of an efficient and clean fuel is in high demand. Hydrogen is a clean, renewable and abundant energy carrier[199] but its large-scale usage is prevented due to the disadvantage of its safe and dense storage in moderate conditions along with fast loading and unloading.[200] Simple storage for hydrogen with its high gravimetric and volumetric density with long life reversible cyclic stability is needed.[169,201] Hence, its storage in molecular form may be more beneficial as compared to the atomic form. Since boron sheets have unique structures with a large distance between the nearest neighbors creating a stable lattice, the molecular hydrogen binds more strongly to boron sheets (0.05 eV) when compared to carbon sheets.[202] Numerous DFT calculations were carried out on boron sheets, which revealed their capacity for hydrogen storage.[202–204] Also, through DFT calculations using VASP, an improvement in the capacity of hydrogen storage was observed in the case of planar borophene and the *ab initio* studies through predicted borophene after doping could be used as one of the potential mediums for hydrogen storage;[154] *i.e.*, when Ca atoms were introduced into boron sheets, the hydrogen storage capacity was improved by 0.20–0.32 eV per H_2 (ref. 154) and it was also observed that the β_{12} borophene phase gave better absorption sites for Ca as it naturally forms hollow hexagons as shown in Fig. 20(l) with an adsorption capacity of 8.92 wt%.[154] When Ca was introduced into the χ^3 phase, the adsorption capacity of H_2 was 7.2%, close to that of graphene.[205,206] A list of hydrogen atom adsorption energies with the capacity of metals decorated on borophene is given in Table 4.

The interaction of a single hydrogen molecule on α-borophene sheet (with adsorption energy of 0.047 eV) was found to be similar to hydrogen interaction with graphene (with adsorption energy of 0.025 eV).[202] Moreover, it was observed that the storage capacity and binding energy of H_2 increased when alkali-metals were dispersed on the sheet of boron (the dispersion of Li on boron and binding of H_2 are represented in Fig. 20(g–k)). Among them, the boron-Li system could contain

 © 2022 The Author(s). Published by the Royal Society of Chemistry

Open Access Article. Published on 21 April 2022. Downloaded on 2/8/2026 10:57:22 PM.
This article is licensed under a Creative Commons Attribution-NonCommercial 3.0 Unported Licence.

Table 4 Previously reported hydrogen storage capacity in weight percentage for different 2D materials when decorated with different metal atoms along with their respective adsorption energies per H_2 molecule

Decorated metal atom	2D material	Structure	Adsorption energy (eV per H_2)	Hydrogen storage capacity (in wt%)	References
Li	Borophene	$\eta = 1/8$	0.23	15.26	207
		β_{12}	0.22	10.85	208
		χ^3	10.39	10.79	133
		α-sheet	0.15	10.75	202
		$\eta = 1/7$	0.35	9.22	209
		2-*Pmmn*	~0.11	6.8	210
	Graphyne	—	0.19	13.0	211
	Graphene	—	0.21	12.8	212
	Silicene	—	0.26	6.35	204
	MoS_2	—	0.20	4.80	213
Na	Borophene	2-*Pmmn*	0.11	9.0	210
		α-sheet	0.07	8.36	202
		χ-h_o	0.15	8.28	214
Ca	Borophene	α-sheet	0.19	12.68	154
		β_{12}	0.24	9.5	153
		2-*Pmmn*	~0.11	7.6	210
		χ^3	0.23	7.2	153
	Graphyne	—	~0.2	~7	215
	BC_7	—	0.26	4.96	216
K	Borophene	α-sheet	0.06	2.39	202

10.7 weight% of the hydrogen molecule with 0.15 eV binding energy, indicating it to be a good template for storing hydrogen.[202] In the previous study, it was observed that Ca could capture 6 hydrogen molecules at 0 K, and when both sides were adsorbed by Ca, its gravimetric density reached 12.68 wt%. Moreover, an increase in temperature along with pressure elevated the performance of hydrogen storage on borophene decorated with Ca.[154]

In one of the very recent research projects on the honeycomb borophene oxide, when decorated with different metals (K, Na and Li), the DFT-d_2 (dispersion corrected) simulations showed that a structure of B_2O decorated with Li achieved a high gravimetric density (8.3 wt% H_2) theoretically, and at saturation, the binding energy of two hydrogen molecules when bound by a single Li gave a binding energy of −0.24 eV per H_2. Born-Oppenheimer Molecular Dynamic (BOMD) simulation at different temperatures showed its stability along with reversibility in its binding of H_2 on Li/B_2O or desorption of hydrogen, which introduced a new form of borophene that could show reversibility in the hydrogen storage as well.[155] Hence, various forms of borophene can be used for storing hydrogen in fuel cell equipped vehicles.

7.3. Sensors

The high mobilities of 2D materials at their monolayer thickness have attracted phosphorene, WS_2, MoS_2, BN and graphene towards sensing applications. However, the deficiency of the electronic bandgap in materials like graphene leads to a lack of high selectivity and sensitivity, indicating its unsuitability for the detection of toxic gases.[3] However, to improve these deficiencies of 2D materials, borophene with metallic structure and enhanced electron density was introduced for vast gas sensing applications as it can adsorb several molecules of gas due to its large surface.[95] In particular, it can be efficiently used as a sensor for toxic gases like NO, CO[157,217] and formaldehyde,[135] as well as non-toxic gases like ethanol[162] and ammonia[130] along with the detection of hydrogen cyanide.[131] Borophenes were also considered to be suitable gas sensors after analysing the electronic and transport properties of edge-hydrogenated borophene through DFT and non-equilibrium Green's function (NEGF).[133]

Theoretical electrochemical studies showed that easier charge transfer between the borophene nanosheets leading to the changing conductivity is one of the conditions favourable for chemical sensors and these can be observed through the band structures and DOS spectrum of borophene nanosheets.[162] On considering this, the adsorption of ethanol was observed through the sharp increment in the current through borophene, indicating that it is an ethanol sensor.[162] Moreover, in B_{36} borophene, electrical signals were generated due to the increase in its electrical conductivity after the adsorption of formaldehyde. This indicated that B_{36} is suitable for the construction of a formaldehyde sensor,[135] and its sensitivity towards different concentrations of HCN indicates B_{36} to be a good sensor for toxic gases. Additionally, it has been reported that for the CO and NO sensors, all fullerenes of boron can be used.[217] Further, after observing the current–voltage, transmission function and the electronic structure of the 2-*Pmmn* phase after the adsorption of NH_3, NO_2, NO and CO, it was studied as a sensor,[138] and a similar phenomenon was observed in the free-standing borophene for a good ammonia sensor.[93] Hence the overall results reported different phases of borophenes acting as sensors for the detection of different gasses. Along with these, the semiconductors such as MoS_2 could also be used as gas sensors for

Open Access Article. Published on 21 April 2022. Downloaded on 2/8/2026 10:57:22 PM.
This article is licensed under a Creative Commons Attribution-NonCommercial 3.0 Unported Licence.

NO molecules when used as substrates for the heterostructures of borophene/MoS_2.[161] Recently, greater efficiency as a sensor was observed in the β_{12} and χ^3 phase when the direct micro-mechanical exfoliation technique was employed for their synthesis because by this method, the resulting sheets of borophene were highly crystalline, due to which there was an enhancement in the purity of chemical phase formation, necessary for an ideal sensor.[103] Moreover, there are other reports on the computational studies on borophene as humidity sensors,[164] metronidazole drug sensor[218] and many other sensors.

7.4. Electrocatalytic applications

Borophene being the lightest 2D nanomaterial can serve as a potential catalyst in the reactions for the evolution of hydrogen (HER),[165,167,169] reduction of oxygen (ORR),[166] the evolution of oxygen (OER)[166] as well as for the electroreduction of CO_2 (CRR).[128,178]

Borophenes show wide applications in the HER. By the method of first principles, it was predicted that borophene, consisting of a basal plane with numerous active sites and exhibiting metallic conductivity with almost free energy could explore the boron monolayers (BMs) as a promising electrocatalyst for the HER.[165] In the case of the χ^3 phase, where the active site is the boron atom with 5-coordinates at S_2 (indicated in Fig. 21(a)), the available free energy as shown in Fig. 21(f) for the adsorption of hydrogen was found to be 0.02 eV, which is much closer to zero when compared to that of platinum[165] with $\Delta G_H = -0.09$ eV (ref. 219) as well as the strong interaction of H atoms with the 2-*Pmmn* phase (Fig. 21(b)) was observed in borophene due to high surface activity. Moreover, the metallic band structure along with numerous active sites in the basal plane of the χ^3 phase indicate its catalytic performance in HER. Similarly, for the β_{12} phase with a 4-coordinated boron atom as an active site, *i.e.*, at its S_1 site (indicated in Fig. 21(c)), the ΔG_H was only 0.1 eV Fig. 21(f) and a small value of ΔG_H was also observed in the β_1 phase and α-sheet as shown in Fig. 21(g) at its S_1 site and S_2 sites, respectively (Fig. 21(d and e)).[165] Nevertheless, all their catalytic performances were not destroyed by Ag substrates.[220] Further, analysis of the effect of substrate, due to the mismatch in charge transfer and strain, showed that the HER performances were positively affected by the substrate.[165]

Furthermore, 2D sheets of boron when synthesized *via* chemical vapor deposition over the molybdenum foils formed an ultrathin film of molybdenum bromide (Mo_3B) and showed its excellent performance as a catalyst in the reaction of hydrogen evolution (HER).[167] However, as MoB_2 consisted of subunits of borophene similar to that of graphene, their catalytic activities were measured with a scan rate of 1 mV s^{-1} for different phases of molybdenum bromide (MoB_2, MoB_2, α-MoB and β-MoB) in a solution of 0.5 M H_2SO_4. In general, the electrocatalytic performances of molybdenum and bromide are very rich when compared to that of carbon. Moreover, the four phases of molybdenum bromide are much better, with a ranking order of MoB_2 > β-MoB > α-MoB > Mo_2B > Mo > B, which indicates the proportionality of electrocatalytic activity with that of the amount of boron as verified from the graph of current density *vs.* potential in Fig. 21(h).[167] The results indicated in Fig. 21(i) for the 1000th cycle in comparison with the 1st cycle revealed excellent performance as a catalyst in the hydrogen evolution reaction even after long-term cycling as compared to that of molybdenum and bromide and their performances are in the order of MoB_2.[167,168]

A series of DFT simulations suggested that a transition metal atom supported by borophane (TM-BH) consisting of vacancies could be efficiently used as an electrocatalyst for the ORR as well as the OER and their corresponding thermodynamic potentials are represented in Fig. 21(j and k). This kind of electrocatalyst can be efficiently used for the technologies of renewable energy.[166] The active reactive sites are generated for the ORR and OER due to the coupling of the transition metal d orbitals with that of the surrounding boron atoms. Among the studied TM-BH the promising electrocatalysts for the ORR were Rh–BH and Fe–BH with an overpotential of 0.47 V and 0.43 V, respectively, whereas an overpotential of 0.24 V was found for Rh–BH, indicating its suitability as an electrocatalyst for the OER.[166] Further, through *ab initio* predictions, a study on borophene after doping with elemental dopants like lithium, sulphur, phosphorous, nitrogen and carbon also proved that the

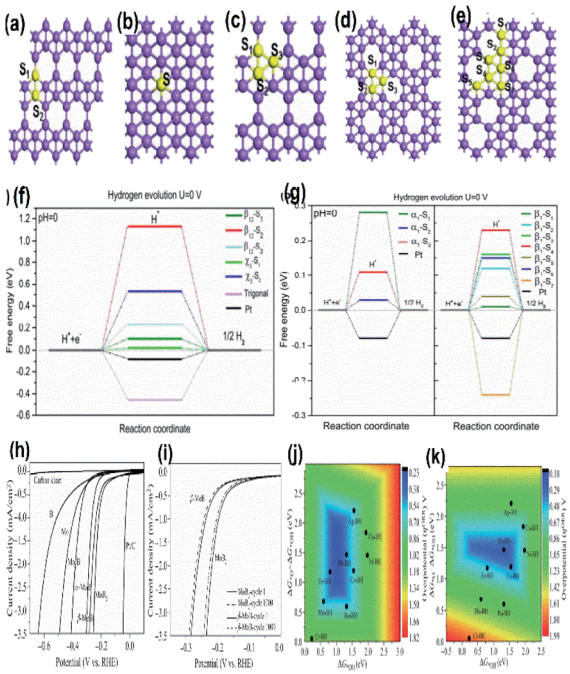

Fig. 21 Crystal structure of the (a) χ^3 phase, (b) 2-*Pmmn* phase, (c) β_{12} phase, (d) α-sheet, (e) β_1 phase of borophene with purple and yellow balls indicating the B atoms. (f and g) HER free energy diagram. (Reproduced from ref. 165 with the permission of the Royal Society of Chemistry). (h) Polarization curves measured in H_2SO_4 (0.5 M) for Pt/C, α-MoB, MoB_2, Mo, B and carbon sheet. (i) CV curves, *i.e.*, stability measurements of MoB_2 and β-MoB for the first and 1000th cycles. (Reproduced from ref. 168 with the permission of John Wiley and Sons). (j and k) Thermodynamic overpotentials of different transition metal-supported borophenes for (j) ORR activity and (k) OER activity of Gibbs free energy. (Reproduced from ref. 166 with the permission of the Royal Society of Chemistry).

© 2022 The Author(s). Published by the Royal Society of Chemistry

Open Access Article. Published on 21 April 2022. Downloaded on 2/8/2026 10:57:22 PM. This article is licensed under a Creative Commons Attribution-NonCommercial 3.0 Unported Licence.

adsorption energies of oxygen and hydrogen were at the top, which subsequently suggested that doped borophene could be used as the catalyst for the evolution reactions of both oxygen and hydrogen.[169] A very recent article explored the catalytic properties of vacancy-containing, carbon-doped borophene towards the OER. They discussed the role of mono-as well as dual-doping of C in β_{12}-borophene, exploring its effect on the π and σ occupancy and reported that boron atoms deficient in charge reduced the binding of oxygen, which reduced the overpotential for the OER.[152]

Reduction of CO_2 into hydrocarbons electrochemically promotes the usage of CO_2, reducing the greenhouse effect. Practically, it is challenging to choose an ideal gas adsorbent material with good selectivity and appropriate adsorbability.[53] More specifically, searching for a highly efficient, metal-free electrocatalyst for the reduction of CO_2 as well as for its storage (energy storage) is still a great challenge. Nevertheless, through a DFT investigation, Qin *et al.*[128] reported that the metallic borophene, free of metal, serves as an efficient electrocatalyst for the reduction of CO_2 to CH_4. The corresponding results indicated that the χ^3 and β_{12} sheets, deficient in electrons, can be given an e^- to activate CO_2 by breaking the π bond. The resulting small value of the activation barrier (0.98 eV) as well as limiting potential (−0.27 V) indicated that the reduction reaction is kinetically and thermodynamically feasible.[128] Further, the theoretical study along with the experiments on the electroreduction of CO_2 by studying the properties of TM-β_{12} as a catalyst showed the stability of this boron monolayer, wherein the initial reduction products for Sc and Ti–Zn were CO and CH_4 with an overpotential of 0.45 V and 0.90 V, respectively, whereas the overpotential for Fe-β_{12} was 0.45 V, thus revealing the reduction mechanism of CO_2 *via* TM-β_{12}.[170] However, this was achieved even on α-borophene when doped with different metals, where the order of increase in the free energy was Co- = Fe- < Pd- < Ni- < Rh- < Ru- < Ir- < Os-doped α borophene. This indicated the very energetic reduction of CO_2 on the α-borophene doped with Co and Pd when compared to the HER.[177] Nevertheless, the newly designed borophene consisting of Cu chains supported on it preferably causes the electroreduction of CO_2 in the following path: $CO_2 \rightarrow COOH^* \rightarrow CO^* \rightarrow CHO^* \rightarrow CH_2O^* \rightarrow CH_3O^* \rightarrow CH_3OH$.[178]

7.5. Optical applications

The features of borophene with its capability of absorption, hybridization, optical modulation[221] along with atomic layer thickness[222] and excellent optical nonlinearity[223] play an important role in photonic and electronic devices. It was reported that in a 2D borophene synthesized *via* liquid -phase exfoliation, when its nonlinear optical properties were measured through Z-scan, the observed saturable absorber (SA) properties indicated that it could serve as an excellent broadband optical switch that could be used for ultrafast mode-locking in mid-infrared and near infrared laser systems. The results further indicated that borophene could also serve as the SA in passively mode locked lasers, as well as future electro-optical applications[223]. Liu *et al.*[222] used critical coupling in the visible wavelength region on the simple structure of borophene to boost the interaction of light-borophene. It was reported that the anisotropic behaviour of borophene could enhance the light absorption of the structure by 99.8% when the polarization-dependent absorption is coupled with guided resonance. The results of this mechanism also indicated that on adjusting the lifetime and carrier density of borophene, the absorption behaviour could be tuned, which could be used for future photonic and electronic devices.[222] Recently, it was reported that the buckled borophene δ_6 exhibits layer-dependent hyperpolarizability and optical absorption and the DFT predictions reflected the anisotropic structural characteristics, indicating the transparency with the weak absorbance of the multilayer borophene. The borophene with a non-centrosymmetric structure indicated an increase in the value of non-zero dipole hyperpolarizability with an increase in the number of layers. Hence, the integration of these properties (*i.e.*, optics, electronics and optoelectronics) could make multilayered borophene a promising candidate in high-performance devices.[224] Zhang *et al.*[221] found that borophene could support the surface plasmon polariton in infrared and visible regimes and hence it could integrate with numerous nanophotonic and optoelectronic devices, which could be further employed as borophene plasmon for the next-generation PoC diagnostic systems.[221] Additionally, improvements in the optical and electronic properties were observed in the ionic liquid interface of hybrid borophene/graphene and this was due to the dramatic changes in the static dielectric constant as a new plasmon frequency appeared in the interface.[225]

8. Summary and outlook

In a very short period, a new 2-dimensional allotrope of boron with much more advanced properties was predicted theoretically *via* DFT calculations, as well as extracted experimentally through MBE, plasma-enhanced CVD, modified Hummers' method and micromechanical exfoliation. It included both substrate-supported borophene and an independent one where all borophene phases showed interesting properties such as high mechanical properties, metallic and sensing properties, negative Poisson's ratio, conductivity and super conducting behaviour. These unique superlative properties could be further altered through strain, carrier doping, altering vacancy concentrations, the formation of heterostructures, *etc.* In this review, the stabilities of different structures were studied with their advantages over other 2D materials and their promising applications. The unique strategy employed by looping the theoretical and experimental results for the material design of borophene rather than direct experimental synthesis has suggested that any element and its compounds could be easily studied in the 2D form to improve the efficiency of synthesis for exploring their desirable properties and discovering new materials.

Despite the advantages of the latest 2D borophene, there are many more challenges for its synthesis and practical application, as shown in Fig. 22. Although there are many theoretical suggestions regarding the properties, only a few have been

Open Access Article. Published on 21 April 2022. Downloaded on 2/8/2026 10:57:22 PM.
This article is licensed under a Creative Commons Attribution-NonCommercial 3.0 Unported Licence.

Fig. 22 Synthesis and application problems faced in general by 2D materials (reprinted with permission from ref. 3. Copyright (2020) Wiley-VCH Verlag GmbH).

experimentally confirmed because the requirement of an atmosphere with ultrahigh vacuum, and their polymorphism in 3D form limit the single-phase synthesis of borophene on a large scale. The employed growth methods are very limited and CVD being harsh and of high-cost produces materials with very small surface areas, whereas a large surface area is key for further applications. However, even though a few top-down methods like micromechanical exfoliation are simple and economical, they were unable to produce atomically layered borophene with uniform thickness. Moreover, the experimental realization of independent borophene is specifically a great challenge, as theories suggest that substrates are necessary for the crystallization of the 2D form of boron since 3D boron crystals are not a van der Waals material. However, most commonly, for their growth, the suggested substrates are metals. Since the borophene interaction is very strong with metallic substrates, a few intrinsic properties (*i.e.*, superconductivity) of β_{12} and χ^3 are affected and their transfer from the metal surface is also a challenging task. Moreover, the electrical shorting nature of the chosen substrate, *i.e.*, metal, renders the transport measurements in borophene.

The rapid progress of borophene is outstanding but the efficient utilization of its high potential is yet to be confirmed. Hence, it can be summarized that along with the growing theoretical suggestions, experimental studies through the large-scale synthesis of borophene on an insulating substrate in high volume are in high demand due to the effective applications. However, conventional techniques employed in the case of graphene could also be used for the synthesis of different phases of borophene, giving rise to a final product with much more advanced properties as compared to graphene and subsequently, many more exotic properties are yet to be experimentally confirmed.

Conflicts of interest

There are no conflicts to declare.

Acknowledgements

S. R. R. acknowledges the UK Engineering and Physical Sciences Research Council (EPSRC) for funding (Grant No. EP/S001395/1).

Notes and references

1 A. K. Geim and K. S. Novoselov, *J. Nanosci. Nanotechnol.*, 2010, 11–19.
2 A. K. Geim, *Phys. Scr.*, 2012, **2012**, 014003.
3 P. Ranjan, J. M. Lee, P. Kumar and A. Vinu, *Adv. Mater.*, 2020, **32**, 2000531.
4 P. Liang, Y. Cao, B. Tai, L. Zhang, H. Shu, F. Li, D. Chao and X. Du, *J. Alloys Compd.*, 2017, **704**, 152–159.
5 M. Novotny, F. J. D. Gutierrez and P. Krstic, *J. Mater. Chem. C*, 2017, **5**, 5426–5433.
6 X. Huang, X. Qi, F. Boey and H. Zhang, *Chem. Soc. Rev.*, 2012, **41**, 666–686.
7 B. Peng, H. Zhang, H. Shao and Y. Xu, *J. Mater. Chem. C*, 2016, **4**, 3592–3598.
8 C. Huo, Z. Yan, X. Song and H. Zeng, *Sci. Bull.*, 2015, **60**, 1994–2008.
9 X. Zhang, L. Huo, A. Ciesielski and P. Samori, *Adv. Energy Mater.*, 2016, **6**, 3523.
10 J. Mao, Y. Wang, Z. Zheng and D. Deng, *Front. Phys.*, 2018, **13**, 1–19.
11 C. Shang, B. Xu, X. Lei, S. Yu, D. Chen, M. Wu, B. Sun, G. Liu and C. Ouyang, *Phys. Chem. Chem. Phys.*, 2018, **20**, 20919–20926.
12 C. R. Dean, A. F. Young, I. Meric, C. Lee, L. Wang, S. Sorgenfrei, K. Watanabe, T. Taniguchi, P. Kim, K. L. Shepard and J. Hone, *Nat. Nanotechnol.*, 2010, **5**, 722–726.
13 L. Li, Y. Yu, G. J. Ye, Q. Ge, X. Ou, H. Wu, D. Feng, X. H. Chen and Y. Zhang, *Nat. Nanotechnol.*, 2014, **9**, 372–377.
14 S. Zhang, Z. Yan, Y. Li, Z. Chen and H. Zeng, *Angew. Chem.*, 2015, **127**, 3155–3158.
15 B. Feng, J. Zhang, Q. Zhong, W. Li, S. Li, H. Li, P. Cheng, S. Meng, L. Chen and K. Wu, *Nat. Chem.*, 2000, **8**, 563–568.
16 Q. H. Wang, K. Kalantar-Zadeh, A. Kis, J. N. Coleman and M. S. Strano, *Nat. Nanotechnol.*, 2012, **7**, 699–712.
17 X.-R. Hu, J.-M. Zheng and Z.-Y. Ren, *Front. Phys.*, 2000, **13**, 1–8.
18 F.-f. Zhu, *et al.*, *Nat. Mater.*, 2015, **14**, 1020–1025.
19 P. Vogt, P. D. Padova, C. Quaresima, J. Avila, E. Frantzeskakis, M. C. Asensio, A. Resta, B. Ealet and G. L. Lay, *Phys. Rev. Lett.*, 2012, **108**, 155501.
20 J. Ji, X. Song, J. Liu, Z. Yan, C. Huo, S. Zhang, M. Su, L. Liao, W. Wang, Z. Ni, Y. Hao and H. Zeng, *Nat. Commun.*, 2016, **7**, 1–9.

© 2022 The Author(s). Published by the Royal Society of Chemistry

Open Access Article. Published on 21 April 2022. Downloaded on 2/8/2026 10:57:22 PM.
This article is licensed under a Creative Commons Attribution-NonCommercial 3.0 Unported Licence.

21 M. Ou, X. Wang, L. Yu, C. Liu, W. Tao, X. Ji and L. Mei, *Adv. Sci.*, 2021, 2001801.
22 N. R. Glavin, R. Rao, V. Varshney, E. Bianco, A. Apte, A. Roy, E. Ringe and P. M. Ajayan, *Adv. Mater.*, 2020, **32**, 1904302.
23 F. R. Fan, R. Wang, H. Zhang and W. Wu, *Chem. Soc. Rev.*, 2021, **50**, 10983–11031.
24 Z. Lin, C. Wang and Y. Chai, *Small*, 2020, **16**, 2003319.
25 S. Xie, W. Yeliang and X. Li, *Adv. Mater.*, 2019, **31**, 1900392.
26 J. Tian, Z. Xu, C. Shen, F. Liu, N. Xu and H. Gao, *Nanoscale*, 2010, **2**, 1375–1389.
27 K. Khan, A. K. Tareen, M. Aslam, M. F. Khan, Z. Shi, C. Ma, S. S. Shams, R. Khatoon, N. Mahmood, H. Zhang and Z. Guo, *Prog. Solid State Chem.*, 2020, **59**, 100283.
28 M. Fujimori, T. Nakata, T. Nakayama, E. Nishibori, K. Kimura, M. Takata and M. Sakata, *Phys. Rev. Lett.*, 1999, **82**, 4452.
29 X. Sun, X. Liu, J. Yin, J. Yu, Y. Li, Y. Hang, X. Zhou, M. Yu, J. Li, G. Tai and W. Guo, *Adv. Funct. Mater.*, 2017, **27**, 1603300.
30 H. Tang and S. Ismail-Beigi, *Phys. Rev. Lett.*, 2007, **99**, 115501.
31 H. Wang, Q. Li, Y. Gao, F. Miao, X. Zho and X. G. Wan, *New J. Phys.*, 2016, **18**, 073016.
32 A. J. Mannix, Z. Zhang, N. P. Guisinger, B. I. Yakobson and M. C. Hersam, *Nat. Nanotechnol.*, 2018, **13**, 444–450.
33 U. Alli, S. Hettiarachchi and S. Kellici, *Chem.–Eur. J.*, 2020, **26**, 6447–6460.
34 C. Liu, X. Huang, Y. Y. Wu, X. Deng, Z. Zheng, Z. Xu and D. Hu, *Nanotechnol. Rev.*, 2021, **10**, 34–49.
35 G. Forte, A. L. Magna, I. Deretzis and R. Pucci, *Nanoscale Res. Lett.*, 2010, **5**, 158–163.
36 X. Liu, Z. Zhang, L. Wang, B. I. Yakobson and M. C. Hersam, *Nat. Mater.*, 2018, **17**, 783–788.
37 Y. Huang, S. N. Shirodkar and B. I. Yakobson, *J. Am. Chem. Soc.*, 2017, **139**, 17181–17185.
38 L. Adamska, S. Sadasivam, J. J. Foley, P. Darancet and S. Sharifzadeh, *J. Phys. Chem. C*, 2018, **122**, 4037–4045.
39 X. Zhou, X. Dong, A. R. Oganov, Q. Zhu, Y. Tian and H. Wang, *Phys. Rev. Lett.*, 2014, **112**, 085502.
40 H. Zhou, Y. Cai, G. Zhang and Y. Zhang, *npj 2D Mater. Appl.*, 2017, **1**, 1–7.
41 H. Zhong, K. Huang, G. Yu and S. Yuan, *Phys. Rev. B*, 2018, **98**, 054104.
42 A. Mogulkoc, Y. Mogulkoc, D. Kecik and E. Durgun, *Phys. Chem. Chem. Phys.*, 2018, **20**, 21043–21050.
43 L. Xu, A. Du and L. Kou, *Phys. Chem. Chem. Phys.*, 2016, **18**, 27284–27289.
44 X. Liu and M. C. Hersam, *Sci. Adv.*, 2019, **5**, eaax6444.
45 A. J. Mannix, X. Zhou, B. Kiraly, J. D. Wood, D. Alducin, B. D. Myers, X. Liu, B. L. Fisher, U. Santiago, J. R. Guest, M. J. Yacaman, A. Ponce, A. R. Oganov, M. C. Hersam and N. P. Guisinger, *Science*, 2015, **350**, 1513–1516.
46 X. Zhang, H. Xie, M. Hu, H. Bao, S. Yue, G. Qin and G. Su, *Phys. Rev. B: Condens. Matter Mater. Phys.*, 2014, **89**, 054310.
47 I. Boustani, *Phys. Rev. B: Condens. Matter Mater. Phys.*, 1997, **55**, 16426.
48 I. Boustani, *Chem. Phys. Lett.*, 1995, **240**, 135–140.
49 I. Boustani, *Surf. Sci.*, 1997, **370**, 355–363.
50 Z. A. Piazza, H. Hu, W. Li, Y. Zhao, J. Li and L. Wang, *Nat. Commun.*, 2014, **5**, 1–6.
51 W. Li, L. Kong, C. Chen, J. Gou, S. Sheng, W. Zhang, H. Li, L. Chen, P. Cheng and K. Wu, *Sci. Bull.*, 2018, **63**, 282–286.
52 A. L. Robinson, *MRS Bull.*, 2017, **42**, 337–338.
53 Z. Xie, X. Meng, X. Li, W. Liang, W. Huang, K. Chen, J. Chen, C. Xing, M. Qiu, B. Zhang, G. Nie, N. Xie, X. Yan and H. Zhang, *Research*, 2020, **2020**, 2624617.
54 C. Hou, G. Tai, Z. Wu and J. Hao, *ChemPlusChem*, 2020, **85**, 2186–2196.
55 I. Boustani, *J. Solid State Chem.*, 1997, **133**, 182–189.
56 A. Quandt and I. Boustani, *ChemPhysChem*, 2005, **6**, 2001–2008.
57 A. Gindulytė, W. N. Lipscomb and L. Massa, *Inorg. Chem.*, 1998, **37**, 6544–6545.
58 I. Matsuda and K. Wu, *2D Boron: Boraphene, Borophene, Boronene*, Springer, 2021.
59 K. C. Lau and R. Pandey, *J. Phys. Chem. C*, 2007, **111**, 2906–2912.
60 D. Li, J. Gao, P. Cheng, J. He, Y. Yin, Y. Hu, L. Chen, Y. Cheng and J. Zhao, *Adv. Funct. Mater.*, 2020, **30**, 1904349.
61 I. Boustani, A. Quandt, E. Hernandez and A. Rubio, *J. Chem. Phys.*, 1999, **110**, 3176–3185.
62 D. Y. Zubarev and A. I. Boldyrev, *Science and Technology of Atomic Molecular, Condensed Matter & Biological Systems Book Series*, 2010, 219–267.
63 X. Yang, Y. Ding and J. Ni, *Phys. Rev. B: Condens. Matter Mater. Phys.*, 2008, **77**, 041402.
64 K. C. Lau, R. Pati, R. Pandey and A. C. Pineda, *Chem. Phys. Lett.*, 2006, **418**, 1105–1110.
65 I. Cabria, J. A. Alonso and M. J. López, *Phys. Status Solidi A*, 2006, **203**, 3523.
66 H. Tang and S. Ismail-Beigi, *Phys. Rev. B: Condens. Matter Mater. Phys.*, 2009, **80**, 134113.
67 Z. Zhang, Y. Yang, E. S. Penev and B. I. Yakobson, *Adv. Funct. Mater.*, 2017, **27**, 1605059.
68 X. Yu, L. Li, X. W. Xu and C. C. Tang, *J. Phys. Chem. C*, 2012, **116**, 20075–20079.
69 C. Ozdogan, S. Mukhopadhyay, W. Hayami, Z. B. Guvenc, R. Pandey and I. Boustani, *J. Phys. Chem. C*, 2010, **114**, 4362–4375.
70 Y. Zhao, S. Zeng and J. Ni, *Appl. Phys. Lett.*, 2016, **108**, 242601.
71 T. R. Galeev, Q. Chen, J. C. Guo, H. Bai, C. Q. Miao, H. G. Lu, A. P. Sergeeva and A. I. Boldyrev, *Phys. Chem. Chem. Phys.*, 2011, **13**, 11575–11578.
72 E. S. Penev, S. Bhowmick, A. Sadrzadeh and B. I. Yakobson, *Nano Lett.*, 2012, **12**, 2441–2445.
73 Y. Wang, J. Lv, L. Zhu and Y. Ma, *Phys. Rev. B: Condens. Matter Mater. Phys.*, 2010, **82**, 094116.
74 X. Wu, j. Dai, Y. Zhao, Z. Zhuo, J. Yang and X. C. Zeng, *ACS Nano*, 2012, **6**, 7443–7453.
75 G. P. Campbell, A. J. Mannix, J. D. Emery, T. L. Lee, N. P. Guisinger, M. C. Hersam and M. J. Bedzyk, *Nano Lett.*, 2018, **18**, 2816–2821.

© 2022 The Author(s). Published by the Royal Society of Chemistry

Open Access Article. Published on 21 April 2022. Downloaded on 2/8/2026 10:57:22 PM.
This article is licensed under a Creative Commons Attribution-NonCommercial 3.0 Unported Licence.

76 Y. Jiao, F. Ma, J. Bell, A. Bilic and A. Du, *Angew. Chem.*, 2016, **128**, 10448–10451.
77 Z. Zhang, E. S. Penev and B. I. Yakobson, *Chem. Soc. Rev.*, 2017, **46**, 6746–6763.
78 L. Kong, K. Wu and L. Chen, *Front. Phys.*, 2018, **13**, 1–11.
79 Y. Zhao, S. Zeng and J. Ni, *Phys. Rev. B*, 2016, **93**, 014502.
80 Y. Liu, E. S. Penev and B. I. Yakobson, *Angew. Chem., Int. Ed.*, 2013, **52**, 3156–3159.
81 Z. Zhang, Y. Yang, G. Gao and B. I. Yakobson, *Angew. Chem.*, 2015, **127**, 13214–13218.
82 H. Liu, J. Gao and J. Zhao, *Sci. Rep.*, 2013, **3**, 1–9.
83 S. Xu, Y. Zhao, J. Liao, X. Yang and H. Xu, *Nano Res.*, 2016, **9**, 2616–2622.
84 Z. Zhang, S. N. Shirodkar, Y. Yang and B. I. Yakobson, *Angew. Chem.*, 2017, **129**, 15623–15628.
85 Y. Yao, F. Ye, X. L. Qi, S. C. Zhang and Z. Fang, *Phys. Rev. B: Condens. Matter Mater. Phys.*, 2007, **75**, 041401.
86 A. N. Kolmogorov and S. Curtarolo, *Phys. Rev. B: Condens. Matter Mater. Phys.*, 2006, **74**, 224507.
87 H. R. Jiang, W. Shyy, M. Liu, Y. X. Ren and T. S. Zhao, *J. Mater. Chem. A*, 2018, **6**, 2107–2114.
88 X. Ji, N. Konh, J. Wang, W. Li, Y. Xiao, S. T. Gan, Y. Zhang, Y. Li, X. Song, Q. Xiong, S. Shi, Z. Li, W. Tao, H. Zhang, L. Mei and J. Shi, *Adv. Mater.*, 2018, **30**, 1803031.
89 J. N. Coleman, *Acc. Chem. Res.*, 2013, **46**, 14–22.
90 Z. Wu, G. Tai, W. Shao, R. Wang and C. Hou, *Nanoscale*, 2020, **12**, 3787–3794.
91 Z. Yan, Z. Peng and J. M. Tour, *Acc. Chem. Res.*, 2014, **47**, 1327–1337.
92 G. Tai, T. Hu, Y. Zhou, X. Wang, J. Kong, T. Zeng, Y. You and Q. Wang, *Angew. Chem., Int. Ed.*, 2015, **54**, 15473–15477.
93 P. Ranjan, T. K. Sahu, R. Bhushan, S. S. R. K. C. Yamijala, D. J. Late, P. Kumar and A. Vinu, *Adv. Mater.*, 2019, **31**, 1900353.
94 L. Zhu, B. Zhao, T. Zhang, G. Chen and S. A. Yang, *J. Phys. Chem. C*, 2019, **123**, 14858–14864.
95 B. Kiraly, X. Liu, L. Wang, Z. Zhang, A. J. Mannix, B. L. Fisher, B. I. Yakobson, M. C. Hersam and N. P. Guisinger, *ACS Nano*, 2019, **13**, 3816–3822.
96 R. Wu, A. Gozar and I. Božović, *npj Quantum Mater.*, 2019, **4**, 1–6.
97 B. Peng, H. Zhang, H. Shao, Z. Ning, Y. Xu, G. Ni, H. Lu, D. W. Zhang and H. Zhu, *Mater. Res. Lett.*, 2017, **5**, 399–407.
98 Z. Wu, G. Tai, R. Liu, C. Hou, W. Shao, X. Liang and Z. Wu, *ACS Appl. Mater. Interfaces*, 2021, **13**, 31808–31815.
99 K. M. Omambac, M. Petrovic, P. Bampoulis, C. Brand, M. A. Kriegel, P. Dreher, D. Janoschka, U. Hagemann, N. Hartmann, P. Valerius, T. Michely, F. J. M. Zu Heringdorf and M. H. Hoegen, *ACS Nano*, 2021, **15**, 7421–7429.
100 N. A. Vinogradov, A. Lyalin, T. Taketsugu, A. S. Vinogradov and A. Preobrajenski, *ACS Nano*, 2019, **13**, 14511–14518.
101 W. Choi, I. Lahiri, R. Seelaboyina and Y. S. Kang, *Crit. Rev. Solid State Mater. Sci.*, 2010, **35**, 52–71.
102 M. Khalkhali, A. Rajabpour and F. Khoeini, *Sci. Rep.*, 2019, **9**, 1–12.
103 S. Chahal, P. Ranjan, M. Motlag, S. S. R. K. C. Yamijala, D. J. Late, E. H. S. Sadki, G. J. Cheng and P. Kumar, *Adv. Mater.*, 2021, **33**, 2102039.
104 T. C. Lebepe, P. Sundararajan and S. O. Oluwatobi, *Nanomaterials*, 2020, **10**, 2149.
105 D. Ayodhya and G. Veerabhadram, *FlatChem*, 2020, **19**, 100150.
106 M. Tatullo, B. Zavan, F. Genovese, B. Codispoti, I. Makeeva, S. Rengo, L. Fortunato and G. Spagnuolo, *Appl. Sci.*, 2019, **9**, 3446.
107 G. I. Giannopoulos, *Comput. Mater. Sci.*, 2017, **129**, 304–310.
108 B. Mortazavi, O. Rahaman, A. Dianat and T. Rabczuk, *Phys. Chem. Chem. Phys.*, 2016, **18**, 27405–27413.
109 V. Wang and W. T. Geng, *J. Phys. Chem. C*, 2017, **121**, 10224–10232.
110 Z. Q. Wang, T. Y. Lu, H. Q. Wang, Y. P. Feng and J. C. Zheng, *Front. Phys.*, 2019, **14**, 1–20.
111 Z. Wang, T. Y. Lu, H. Q. Wang, Y. P. Feng and J. C. Zheng, *Phys. Chem. Chem. Phys.*, 2016, **18**, 31424–31430.
112 R. Peköz, M. Konuk, M. E. Kilic and E. Durgun, *ACS Omega*, 2018, **3**, 1815–1822.
113 J. He, D. Li, Y. Ying, C. Feng, J. He, C. Zhong, H. Zhou, P. Zhou and G. Zhang, *npj Comput. Mater.*, 2019, **5**, 1–8.
114 C. Hou, G. Tai, J. Hao, L. Sheng, B. Liu and Z. Wu, *Angew. Chem.*, 2020, **132**, 10911–10917.
115 Q. Wei and X. Peng, *Appl. Phys. Lett.*, 2014, **104**, 251915.
116 J. H. Liao, Y. C. Zhao, Y. J. Zhao, H. Xu and X. B. Yang, *Phys. Chem. Chem. Phys.*, 2017, **19**, 29237–29243.
117 H. Liu, A. T. Neal, Z. Zhu, Z. Luo, X. Xu, D. Tománek and P. D. Ye, *ACS Nano*, 2014, **8**, 4033–4041.
118 J. Kunstmann and A. Quandt, *Phys. Rev. B: Condens. Matter Mater. Phys.*, 2006, **74**, 035413.
119 I. Boustani and A. Quandt, *Comput. Mater. Sci.*, 1998, **11**, 132–137.
120 Y. Wang, X. Jiang, Y. Wang and J. Zhao, *Phys. Chem. Chem. Phys.*, 2021, **23**, 17150–17157.
121 W. Shao, G. Tai, C. Hou, Z. Wu, Z. Wu and X. Liang, *ACS Appl. Electron. Mater.*, 2021, **3**, 1133–1141.
122 W. Hu, N. Qin, G. Wu, Y. Lin, S. Li and D. Bao, *J. Am. Chem. Soc.*, 2012, **134**, 14658–14661.
123 Z. Q. Wang, T. Y. Lu, H. Q. Wang, Y. P. Feng and J. C. Zheng, *RSC Adv.*, 2017, **7**, 47746–47752.
124 Y. Zhang, Z. F. Wu, P. F. Gao, S. Zhang and Y. H. Wen, *ACS Appl. Mater. Interfaces*, 2016, **8**, 22175–22181.
125 J. Yu, M. Zhou, M. Yang, Q. Yang, Z. Zhang and Y. Zhang, *ACS Appl. Energy Mater.*, 2020, **3**, 11699–11705.
126 J. Khanifaev, R. Pekoz, M. Konuk and E. Durgun, *Phys. Chem. Chem. Phys.*, 2017, **19**, 28963–28969.
127 J. Li, X. Chen, Z. Yang, X. Liu and X. Zhang, *J. Mater. Chem. C*, 2021, **9**, 1069–1076.
128 Q. Sun, G. Qin, Q. Cui and A. Du, *ChemCatChem*, 2020, **12**, 1483–1490.
129 H. Kim and H. N. Alshareef, *ACS Mater. Lett.*, 2019, **2**, 55–70.
130 Z. Rostami and H. Soleymanabadi, *J. Mol. Model.*, 2016, **22**, 70.
131 O. Akbar, *Comput. Theor. Chem.*, 2017, **1115**, 179–184.
132 D. O. Lindroth and P. Erhart, *Phys. Rev. B*, 2016, **94**, 115205.

© 2022 The Author(s). Published by the Royal Society of Chemistry

Open Access Article. Published on 21 April 2022. Downloaded on 2/8/2026 10:57:22 PM. This article is licensed under a Creative Commons Attribution-NonCommercial 3.0 Unported Licence.

133 V. Shukla, J. Warna, N. K. Jena, A. Grigoriev and R. Ahuja, *J. Phys. Chem. C*, 2017, **121**, 26869–26876.
134 T. Liu, Y. Chen, M. Zhang, L. Yuan, C. Zhang, J. Wang and J. Fan, *AIP Adv.*, 2017, **7**, 125007.
135 A. S. Kootenaei and G. Ansari, *Phys. Lett. A*, 2016, **380**, 2664–2668.
136 A. Rastgou, H. Soleymanabadi and A. Bodaghi, *Microelectron. Eng.*, 2017, **169**, 9–15.
137 A. Lherbier, A. R. Botello-Méndez and J. C. Charlier, *2D Materials*, 2016, **3**, 045006.
138 C. S. Huang, A. Murat, V. Babar, E. Montes and U. Schwingenschlogl, *J. Phys. Chem. C*, 2018, **122**, 14665–14670.
139 S. Kumar, M. Singh, D. K. Sharma and S. Aulucl, *Comput. Condens. Matter*, 2020, **22**, e00436.
140 H. Sun, Q. Li and X. G. Wan, *Phys. Chem. Chem. Phys.*, 2016, **18**, 14927–14932.
141 Y. Hu, Y. Yin, S. Li, H. Zhou, D. Li and G. Zhang, *Nano Lett.*, 2020, **20**, 7619–7626.
142 B. Mortazavi, M. Q. Le, T. Rabczuk and L. F. C. Pereira, *Phys. E*, 2017, **93**, 202–207.
143 B. Y. Shapiro, I. Shapiro, D. Li and B. Rosenstein, *J. Phys.: Condens. Matter*, 2018, **30**, 335403.
144 J. Chapman, Y. Su, C. A. Howard, D. Kundys, A. N. Grigorenko, F. Guinea, A. K. Geim, I. V. Grigorieva and R. R. Nair, *Sci. Rep.*, 2016, **6**, 1–6.
145 E. S. Penev, A. Kutana and B. I. Yakobson, *Nano Lett.*, 2016, **16**, 2522–2526.
146 J. C. Zheng and Y. Zhu, *Phys. Rev. B: Condens. Matter Mater. Phys.*, 2006, **73**, 024509.
147 R. C. Xiao, D. F. Shao, W. J. Lu, H. Y. Lv, J. Y. Li and Y. P. Sun, *Appl. Phys. Lett.*, 2016, **109**, 122604.
148 Y. Wang, Y. Park, L. Qiu, I. Mitchell and F. Ding, *J. Phys. Chem. Lett.*, 2020, **11**, 6235–6241.
149 R. R. Zope and T. Baruah, *Chem. Phys. Lett.*, 2011, **501**, 193–196.
150 M. J. van Setten, M. A. Uijttewaa, G. A. de Wijs and R. A. de Groot, *J. Am. Chem. Soc.*, 2007, **129**, 2458–2465.
151 R. C. Andrew, R. E. Mapasha, A. M. Ukpong and N. Chetty, *Phys. Rev. B: Condens. Matter Mater. Phys.*, 2012, **85**, 125428.
152 E. S. Erakulan and R. Thapa, *Appl. Surf. Sci.*, 2022, **574**, 151613.
153 X. Chen, L. Wang, W. Zhang, J. Zhang and Y. Yuan, *Int. J. Hydrogen Energy*, 2017, **42**, 20036–20045.
154 J. Wang, Y. Du and L. Sun, *Int. J. Hydrogen Energy*, 2016, **41**, 5276–5283.
155 P. Habibi, T. J. H. Vlugt, P. Dey and O. A. Moultos, *ACS Appl. Mater. Interfaces*, 2021, **13**, 43233–43240.
156 L. Kou, T. Frauenheim and C. Chen, *J. Phys. Chem. Lett.*, 2014, **5**, 2675–2681.
157 O. Leenaerts, B. Partoens and F. M. Peeters, *Phys. Rev. B: Condens. Matter Mater. Phys.*, 2008, **77**, 125416.
158 B. Feng, J. Zhang, R. Y. Liu, T. Iimori, C. Lian, H. Li, L. Chen, K. Wu, S. Meng, F. Komori and I. Matsuda, *Phys. Rev. B*, 2016, **94**, 041408.
159 Y. An, J. Jiao, Y. Hou, H. Wang, D. Wu, T. Wang, Z. Fu, G. Xu and R. Wu, *Phys. Chem. Chem. Phys.*, 2018, **20**, 21552–21556.
160 B. Feng, Z. Ding, S. Meng, Y. Yao, X. He, P. Cheng, L. Chen and K. Wu, *Nano Lett.*, 2012, **12**, 3507–3511.
161 J. Shen, Z. Yang, Y. Wang, L. C. Xu, R. Liu and X. Liu, *Appl. Surf. Sci.*, 2020, **504**, 144412.
162 V. Nagarajan and R. Chandiramouli, *Comput. Theor. Chem.*, 2017, **1105**, 52–60.
163 M. Z. M. Nasir and M. Pumera, *TrAC, Trends Anal. Chem.*, 2019, **121**, 115696.
164 C. Hou, G. Tai, B. Liu, Z. Wu and Y. Yin, *Nano Res.*, 2020, 1–8.
165 L. Shi, C. Ling, Y. Ouyang and J. Wang, *Nanoscale*, 2017, **9**, 533–537.
166 Y. Singh, S. Back and Y. Jung, *Phys. Chem. Chem. Phys.*, 2018, **20**, 21095–21104.
167 X. Wang, G. Tai, Z. Wu, T. Hu and R. Wang, *J. Mater. Chem. A*, 2017, **5**, 23471–23475.
168 H. Park, A. Encinas, J. P. Scheifers, Y. Zhang and B. P. Fokwa, *Angew. Chem., Int. Ed.*, 2017, **56**, 5575–5578.
169 S. H. Mir, S. Chakraborty, P. C. Jha, J. Warna, H. Soni, P. K. Jha and R. Ahuja, *Appl. Phys. Lett.*, 2016, **109**, 053903.
170 J. H. Liu, L. M. Yang and E. Ganz, *RSC Adv.*, 2019, **9**, 27710–27719.
171 L. Zhang, P. Liang, H. Shu, X. L. Man, F. Li, J. Huang, Q. Dong and D. Chao, *J. Phys. Chem. C*, 2017, **121**, 15549–15555.
172 M. Makaremi, B. Mortazavi and C. V. Singh, *Mater. Today Energy*, 2018, **8**, 22–28.
173 B. Mortazavi, O. Rahaman, S. Ahzi and T. Rabczuk, *Appl. Mater. Today*, 2017, **8**, 60–67.
174 Z. L. Lv, H. L. Cui, H. Wang and X. H. Li, *Appl. Surf. Sci.*, 2021, **562**, 150154.
175 S. Göktuna and N. Taşaltın, *Phys. E*, 2021, **134**, 114833.
176 O. Folorunso, Y. Hamam, R. Sadiku, S. S. Ray and G. J. Adekoya, *FlatChem*, 2021, **26**, 100211.
177 X. Xu, X. Hou, J. Lu, P. Zhang, B. Xiao and J. Mi, *J. Phys. Chem. C*, 2020, **124**, 24156–24163.
178 H. Shen, Y. Li and Q. Sun, *Nanoscale*, 2018, **10**, 11064–11071.
179 H. S. Kim and Y. H. Kim, *Biosens. Bioelectron.*, 2015, **69**, 186–198.
180 M. Raoof, K. Jans, G. Bryce, S. Ebrahim, L. Lagae and A. Witvrouw, *Microelectron. Eng.*, 2013, **111**, 421–424.
181 A. M. Attaran, S. A. Manafi, M. Javanbakht and M. Enhessari, *J. Nanostruct. Chem.*, 2016, **6**, 121–128.
182 A. L. Petranovska, N. V. Abramov, S. P. Turanska, P. P. Gorbyk, A. N. Kaminskiy and N. V. Kusyak, *J. Nanostruct. Chem.*, 2015, **3**, 275–285.
183 J. Fang, H. Nakamura and H. Maeda, *Adv. Drug Delivery Rev.*, 2011, **63**, 136–151.
184 K. Bhise, S. K. Kashaw, S. Sau and A. K. Iyer, *Int. J. Pharm.*, 2017, **526**, 1–2.
185 M. Fan, Y. Wen, D. Ye, Z. Jin, P. Zhao, D. Chen, X. Lu and Q. He, *Adv. Healthcare Mater.*, 2019, **8**, 1970054.
186 H. Nishino, T. Fujita, A. Yamamoto, T. Fujimori, A. Fujino, S. I. Ito, J. Nakamura, H. Hosono and T. Kondo, *J. Phys. Chem. C*, 2017, **121**, 10587–10593.

© 2022 The Author(s). Published by the Royal Society of Chemistry

Open Access Article. Published on 21 April 2022. Downloaded on 2/8/2026 10:57:22 PM. This article is licensed under a Creative Commons Attribution-NonCommercial 3.0 Unported Licence.

187 N. K. Prasad, K. Rathinasamy, D. Panda and D. Bahadur, *J. Mater. Chem.*, 2007, **17**, 5042–5051.
188 W. Tao, N. Kong, X. Ji, Y. Zhang, A. Sharma, J. Ouyang, B. Qi, J. Wang, N. Xie, C. Kang, H. Zhang, O. C. Farokhzad and J. S. Kim, *Chem. Soc. Rev.*, 2019, **48**, 2891–2912.
189 H. R. Jiang, Z. Lu, M. C. Wu, F. Ciucci and T. S. Zhao, *Nano Energy*, 2016, **23**, 97–104.
190 C. Liu, F. Li, L. P. Ma and H. M. Cheng, *Adv. Mater.*, 2010, **22**, E28–E62.
191 J. Yan, Q. Wang, T. Wei and Z. Fan, *Adv. Energy Mater.*, 2014, **4**, 1300816.
192 Y. Han, Y. Ge, Y. Chao, C. Wang and G. G. Wallance, *J. Energy Chem.*, 2018, **27**, 57–72.
193 C. Lu, Y. Yang and X. Chen, *Nano Lett.*, 2019, **19**, 4103–4111.
194 H. Li, L. Jing, W. Liu, J. Lin, R. Y. Tay, S. H. Tsang and E. H. T. Teo, *ACS Nano*, 2018, **12**, 1262–1272.
195 P. Kerativitayanan, M. Tatullo, M. Khariton, P. Joshi, B. Perniconi and A. K. Gaharwar, *ACS Biomater. Sci. Eng.*, 2017, **3**, 590–600.
196 D. Y. Yeom, W. Jeon, N. D. K. Tu, S. Y. Yeo, S. S. Lee, B. J. Sung, H. Chang, J. A. Lim and H. Kim, *Sci. Rep.*, 2015, **5**, 1–10.
197 S. Saha, M. Jana, P. Khanra, P. Samanta, H. Y. Koo, N. C. Murmu and T. Kuila, *ACS Appl. Mater. Interfaces*, 2015, **7**, 14211–14222.
198 T. Wu, X. Wu, L. Li, M. Hao, G. Wu, T. Zhang and S. Chen, *Angew. Chem., Int. Ed.*, 2020, **59**, 23800–23809.
199 R. Coontz and B. Hanson, *Science*, 2004, **305**, 957.
200 L. Schlapbach, and A. Züttel, *Materials for sustainable energy: a collection of peer-reviewed research and review articles from nature publishing group*, 2011, pp. 265–270.
201 Y. Wang, J. Fan and M. Trenary, *Chem. Mater.*, 1993, **5**, 192–198.
202 S. Er, G. A. de Wijs and G. Brocks, *J. Phys. Chem. C*, 2009, **113**, 18962–18967.
203 A. Lebon, R. H. Aguilera-del-Toro, L. J. Gallego and A. Vega, *Int. J. Hydrogen Energy*, 2019, **44**, 1021–1033.
204 L. Yuan, L. Kang, Y. Chen, D. Wang, J. Gong, C. Wang, M. Zhang and X. Wu, *Appl. Surf. Sci.*, 2018, **434**, 843–849.
205 V. Tozzini and V. Pellegrini, *Phys. Chem. Chem. Phys.*, 2013, **15**, 80–89.
206 J. Shang, Y. Ma, Y. Gu and L. Kou, *Phys. Chem. Chem. Phys.*, 2018, **20**, 28964–28978.
207 J. Li, H. Zhang and G. Yang, *J. Phys. Chem. C*, 2015, **119**, 19681–19688.
208 T. Liu, Y. Chen, H. Wang, M. Zhang, L. Yuan and C. Zhang, *Materials*, 2017, **10**, 1399.
209 Y. S. Wang, F. Wang, M. Li, B. Xu, Q. Sun and Y. Jia, *Appl. Surf. Sci.*, 2012, **258**, 8874–8879.
210 S. Haldar, S. Mukherjee and C. V. Singh, *RSC Adv.*, 2018, **8**, 20748–20757.
211 B. Xu, X. L. Lei, G. Liu, M. S. Wu and C. Y. Ouyang, *Int. J. Hydrogen Energy*, 2014, **39**, 17104–17111.
212 C. Ataca, E. Akturk, S. Ciraci and H. Ustunel, *Appl. Phys. Lett.*, 2008, **93**, 043123.
213 C. Zhang, S. Tang, M. Deng and Y. Du, *Chin. Phys. B*, 2018, **27**, 066103.
214 Y. F. Zhang and X. L. Cheng, *Phys. E*, 2019, **107**, 170–176.
215 H. J. Hwang, Y. Kwon and H. Lee, *J. Phys. Chem. C*, 2012, **116**, 20220–20224.
216 X. L. Lei, G. Liu, M. S. Wu, B. Xu, C. Y. Ouyang and B. C. Pan, *Int. J. Hydrogen Energy*, 2014, **39**, 2142–2148.
217 R. Chandiramouli and V. Nagarajan, *Vacuum*, 2017, **142**, 13–20.
218 C. Xiao, K. Ma, G. Cai, X. Zhang and E. Vessally, *J. Mol. Graphics Modell.*, 2020, **96**, 107539.
219 J. K. Nørskov, T. Bligaard, A. Logadottir, J. R. Kitchin, J. G. Chen, S. Pandelov and U. Stimming, *J. Electrochem. Soc.*, 2005, **152**, J23.
220 C. Liu, Z. Dai, J. Zhang, Y. Jin, D. Li and C. Sun, *J. Phys. Chem. C*, 2018, **122**, 19051–19055.
221 J. Zhang, Z. Zhang, X. Song, H. Zhang and J. Yang, *Nanomaterials*, 2021, **11**, 1165.
222 T. Liu, C. Zhou and S. Xiao, *Opt. Express*, 2021, **29**, 8941–8950.
223 C. Ma, P. Yin, K. Khan, A. K. Tareen, R. Huang, J. Du, Y. Zhang, Z. Shi, R. Cao, S. Weiand and X. Wang, *Small*, 2021, **17**, 2006891.
224 G. Sachdeva, S. Kaur, R. Pandey and S. P. Karna, *Computation*, 2021, **9**, 101.
225 K. Zhour, J. M. Otero-Mato, F. E. H. Hassan, H. Fahs, M. Vaezzadeh, E. López-Lago, L. J. Gallego and L. M. Varela, *J. Mol. Liq.*, 2021, **321**, 114759.

© 2022 The Author(s). Published by the Royal Society of Chemistry